Intestinal epithelial cell autophagy is required to protect against TNF-induced apoptosis during chronic colitis in mice

Johanna Pott[1], Agnieszka Martyna Kabat[1,2], Kevin Joseph Maloy[1*]

[1]Sir William Dunn School of Pathology, University of Oxford, Oxford, UK.
[2]Current address: Max Planck Institute of Immunobiology and Epigenetics, Freiburg, Germany

* Lead Contact:
Kevin Maloy
Sir William Dunn School of Pathology
University of Oxford
South Parks Road
Oxford, Ox1 3RE, UK
Email: kevin.maloy@path.ox.ac.uk
Phone: +44 (0)1865 275572

Running title: Epithelial autophagy dampens chronic colitis.

Summary

Genome-wide association studies have linked polymorphisms in the autophagy gene *ATG16L1* with susceptibility to inflammatory bowel disease (IBD). However, the cell-type specific effects of autophagy on the regulation of chronic intestinal inflammation have not been investigated. Here, we assessed the effect of myeloid-specific or intestinal epithelial cell (IEC)-specific deletion of *Atg16l1* on chronic colitis triggered by the intestinal opportunistic pathogen *Helicobacter hepaticus* in mice. Although *Atg16l1*-deficiency in myeloid cells had little effect on disease, mice selectively lacking *Atg16l1* in IEC (*Atg16l1*^{VC}) developed severely exacerbated pathology, accompanied by elevated pro-inflammatory cytokine secretion and increased IEC apoptosis. Using *ex vivo* IEC organoids, we demonstrate that autophagy intrinsically controls TNF-induced apoptosis and *in vivo* blockade of TNF attenuated the exacerbated pathology in *Atg16l1*^{VC} mice. These findings suggest that the IBD susceptibility gene *ATG16L1* and the process of autophagy within the epithelium controls inflammation-induced apoptosis and barrier integrity to limit chronic intestinal inflammation.

Introduction

Inflammatory bowel disease (IBD) is a chronic inflammatory disorder with unknown etiology, with two main clinical forms – Crohn's disease (CD) and ulcerative colitis (UC). Although there are broadly conserved features of intestinal immunopathology that present in IBD patients, including dysregulated immune responses, aberrant cytokine secretion, and alterations in barrier function and intestinal microbiota (Maloy and Powrie, 2011; Neurath, 2014), the clinical manifestations are heterogeneous (Lonnfors et al., 2014). The heterogeneous nature of IBD is further emphasized by genome wide association studies (GWAS) that have identified many pathways that potentially contribute to the pathogenesis of IBD (Jostins et al., 2012; Liu et al., 2015), and which allow further stratification of patients, besides disease manifestations and immunological profiling (de Souza et al., 2017). Much current IBD research focuses on unraveling the mechanistic effects of genes and pathways that have been implicated by GWAS. A better understanding of how host genetics control disease development and progression should enable treatments to be utilized in more effective and cost-efficient manner. Current treatment options for IBD include, anti-inflammatory and immune-suppressive drugs, surgery, and biologics that specifically target the dysregulated immune response (Chang and Hanauer, 2017). In the latter category, anti-TNF treatment has high efficacy and has been increasingly employed, however 40 % of IBD patients do not respond to this therapy and many become refractory to treatment (Cohen and Sachar, 2017; Hendy et al., 2016). As it is not fully understood how anti-TNF treatment acts and which cell types are targeted, it is difficult to predict which patients are most likely to benefit and what mechanisms prevent responsiveness.

Polymorphisms in *ATG16L1* and other autophagy genes suggest an important role of autophagy in IBD pathogenesis (Hampe et al., 2007; Rioux et al., 2007). *ATG16L1* is an essential autophagy gene and the *T300A* polymorphism that shows the strongest link to IBD development results in destabilization of the protein, facilitating caspase 3 dependent degradation during cellular stress (Mizushima et al., 2011; Murthy et al., 2014). Autophagy is a conserved intracellular degradation pathway that facilitates maintenance of cellular homeostasis during periods of stress or malnutrition, but it also impacts on many pathways of cellular immune defense (Kabat et al., 2016b). The ubiquitous nature of autophagy and its interactions with many other essential homeostatic cellular processes makes it difficult to unravel precisely how disease-associated polymorphisms can predispose to IBD. Nevertheless, several studies have described cell-type specific functions of autophagy in the context of mucosal homeostasis (Adolph et al., 2013; Cadwell et al., 2008; Kabat et al., 2016a; Kabat et al., 2016b; Saitoh et al., 2008). In myeloid cells autophagy is implicated in regulation of the proinflammatory cytokine response, particularly secretion of inflammasome dependent cytokines and ROS levels are increased in autophagy-deficient macrophages (Lassen et al., 2014; Saitoh et al., 2008; Zhang et al., 2017). Bone-marrow chimeric mice with autophagy-deficient haematopoetic cells, *Atg16l1*-hypomorphic mice or mice lacking *Atg16l1* in the myeloid compartment all show increased pathology in the chemically induced model of DSS colitis (Cadwell et al., 2010; Saitoh et al., 2008; Zhang et al., 2017). Although autophagy enhances killing of *Salmonella* by DCs and macrophages *in vitro*, how much this impacts on disease development during infection is less clear (Conway et al., 2013; Thurston et al., 2012; Zhang et al., 2017). Recent studies also

97 revealed that autophagy in T cells is required for the maintenance of intestinal
98 homeostasis, as Treg cells rely on autophagy for their survival and function in
99 the gut (Kabat et al., 2016a; Wei et al., 2016). Autophagy has also been reported
100 to regulate many key functions of intestinal epithelial cells (IEC). Autophagy has
101 been shown to influence granule structure of goblet and Paneth cells (secretory
102 cells of the intestinal epithelium) under stressed conditions, such as during
103 norovirus infection or ER stress (Adolph et al., 2013; Cadwell et al., 2010; Lassen
104 et al., 2014; Patel et al., 2013). Epithelial autophagy has also been implicated in
105 barrier enforcement during *Salmonella* infection, as autophagy-deficiency of IEC
106 led to increased bacterial dissemination and inflammation (Benjamin et al.,
107 2013; Conway et al., 2013; Lassen et al., 2014).
108 Taken together, these studies indicate that autophagy has wide-ranging
109 functional effects on various cell types that could potentially regulate
110 inflammatory responses. However, thus far, there have been few comparative
111 studies of the cell-type specific effects of autophagy on the regulation of chronic
112 intestinal inflammation. Here, we have undertaken a comprehensive analysis of
113 the consequences of autophagy deficiency within different cellular
114 compartments on chronic intestinal pathology. We have utilized a well-
115 characterized mouse IBD model in which chronic intestinal inflammation is
116 induced by infection with the gram negative enteric bacterium *Helicobacter*
117 *hepaticus* together with concomitant blockade of immune regulatory circuits
118 using anti-IL10R (Kullberg et al., 2006). Our previous work has shown that this
119 model recapitulates several features of chronic intestinal pathology found in IBD
120 patients, that pathology is driven by similar excessive innate and adaptive
121 immune responses, and that disease is controlled by the same key pro-

inflammatory mediators (Hue et al., 2006; Kullberg et al., 2006; Maloy et al., 2003; Schiering et al., 2014; West et al., 2017). We find that selective autophagy deficiency in myeloid cells only marginally affects colitis development, whereas autophagy deficiency in IEC results in severely exacerbated pathology. We further show that autophagy regulates cytokine-induced apoptosis in IEC and blockade of TNF attenuates chronic colitis in IEC-specific *Atg16l1*-deficient mice by ameliorating epithelial apoptosis.

Results

Autophagy-deficiency in intestinal epithelial cells (IEC) predisposes to chronic colitis

To analyze the cell-type specific role of autophagy in chronic intestinal inflammation, we crossed *Atg16l1*$^{fl/fl}$ mice (Hwang et al., 2012) with strains expressing Cre recombinase under the control of various cell-type specific promoters. Thus, we generated transgenic mice lacking *Atg16l1* in neutrophils/macrophages (*Atg16l1*^{LysM}), in dendritic cells (*Atg16l1*^{CD11c}) or in IEC (*Atg16l1*^{VC}). Analyses of *Atg16l1* expression by quantitative PCR confirmed that LysM-Cre and CD11c-Cre driven recombination selectively reduced expression of *Atg16l1* in myeloid cell compartments (CD11c$^+$, MHC2$^+$, CD45$^+$ DC and CD64$^+$, CD11b$^+$, CD45$^+$ macrophages), whereas Villin-Cre driven recombination selectively ablated *Atg16l1* expression in IEC (Fig. S1 A-C).

Intestinal inflammation was induced by oral infection with *Helicobacter hepaticus* and blockade of the regulatory response with anti-IL10R antibody (Kullberg et al., 2006)(Fig. 1 A). To exclude any potential microbiota differences, the transgenic lines were bred as heterozygous for the *Cre* allele, allowing experimental groups to be set up using littermate controls (*Atg16l1*$^{fl/fl}$) that were co-housed throughout the experiment.

At two weeks after colitis induction, assessment of histopathology of the caecum and colon revealed slightly elevated pathology in *Atg16l1*^{CD11c} and *Atg16l1*^{LysM} mice compared to *Atg16l1*$^{fl/fl}$ mice, but these differences were not statistically significant (Fig. 1 B, C). Comparison with the concurrent littermate controls confirmed that there was only a minor increase in pathology and revealed no

significant alterations within the lamina propria CD4$^+$ T cell compartments in either *Atg16l1*^{CD11c} or *Atg16l1*^{LysM} mice (Fig. S1 D-K).

In contrast, *Atg16l1*^{VC} mice showed significantly elevated histopathology in both the caecum and colon at 2 weeks and 4 weeks after colitis induction (Fig. 1 B - G). Although overall disease severity varied slightly between experiments, we consistently observed significantly increased histopathology in *Atg16l1*^{VC} mice compared to their *Atg16l1*$^{fl/fl}$ littermates. This was in accordance with increased weight loss in the *Atg16l1*^{VC} mice (Fig. 1 H) and increased numbers of CD4$^+$ T cells in the lamina propria compared to *Atg16l1*$^{fl/fl}$ littermates (Fig. 1 I). Furthermore, secretion of inflammatory cytokines, such as TNF, IFN-γ and IL1-β, by colon explants isolated from *Atg16l1*^{VC} mice were significantly elevated at 2 weeks after colitis induction compared to explants obtained from *Atg16l1*$^{fl/fl}$ littermates (Fig. 1 J-L). However, frequencies of CD4$^+$ T effector and Treg subsets in the lamina propria and *H.h.* colonization levels were not altered in the *Atg16l1*^{VC} mice relative to their *Atg16l1*$^{fl/fl}$ littermates (Fig. S2). We also tested the role of intestinal epithelial autophagy in a model of acute intestinal infection using oral infection with *Citrobacter rodentium* (Collins et al., 2014). We found that *Citrobacter rodentium* infection induced comparable levels of intestinal pathology in *Atg16l1*^{VC} mice and *Atg16l1*$^{fl/fl}$ mice (Fig. S3 A, B, E, F), which was in accordance with similar bacterial colonization levels (Fig. S3 C, D). Taken together, these data reveal that autophagy within IEC exerts a protective effect during *Helicobacter hepaticus*-triggered chronic colitis, whereas autophagy in myeloid cell compartments (CD11c$^+$ or LysM$^+$ cells) plays only a marginal role. Therefore, we focused our further analyses on the consequences of autophagy

impairment in IEC and the impact that it has on the development of chronic colitis.

Autophagy does not regulate chemokine expression or ER stress induction in IEC

We next sought to analyze how autophagy-deficiency within the epithelium influences colitis development. First, we noticed that *in vivo* IEC from *Atg16l1*^{VC} mice expressed elevated levels of chemokines *Cxcl2* and *Cxcl5* at 2 weeks and 4 weeks after colitis induction (Fig. 2 A, B).

To analyze whether the chemokine response of the epithelium is intrinsically controlled by autophagy, we employed the *ex vivo* organoid system to grow primary IEC from either *Atg16l1*$^{fl/fl}$ or *Atg16l1*^{VC} mice (Heijmans et al., 2013). Western blot analysis of LC3 lipidation confirmed autophagy deficiency in IEC organoids derived from *Atg16l1*^{VC} mice (Fig. 2 D). In the presence of complete medium containing the essential IEC growth factors (Wnt3a, R-spondin and noggin), we found that autophagy-deficient colonic IEC proliferated and formed organoids that were morphologically indistinguishable from wild type organoids.

To mimic the conditions present in the inflamed intestine, we isolated lamina propria leucocytes (LPL) from colitic mice (WT mice subjected to *H.h.* + αIL10R treatment for 2 weeks) and cultured them overnight to generate inflammatory conditioned medium (iCM) that was harvested from the culture supernatant. We then stimulated *Atg16l1*$^{fl/fl}$ or *Atg16l1*^{VC} IEC organoids with 10% iCM to assess IEC responses to the colitic microenvironment. We found that both *Atg16l1*$^{fl/fl}$ and *Atg16l1*^{VC} IEC responded to stimulation with iCM, as evidenced by rapid

phosphorylation and nuclear translocation of Stat3 (Fig. 2 C, D). Western blot analysis also confirmed robust and equivalent activation of the intracellular Map kinase pathway in response to iCM stimulation in both *Atg16l1*$^{fl/fl}$ and *Atg16l1*^{VC} IEC (Fig. 2 D). In addition, *Cxcl2* and *Cxcl5* expression were induced to comparable levels in *Atg16l1*$^{fl/fl}$ and *Atg16l1*^{VC} organoids after 6h of stimulation with iCM (Fig. 2 E, F).

In order to test the response of primary IEC from *Atg16l1*$^{fl/fl}$ or *Atg16l1*^{VC} mice to bacterial stimulation, we adapted the primary IEC culture system to generate polarized monolayers (Moon et al., 2013). Thus, IEC organoids from *Atg16l1*$^{fl/fl}$ or *Atg16l1*^{VC} mice were seeded as monolayers and subsequently infected with *H. hepaticus* at the apical surface. Autophagy deficiency of the IEC monolayer derived from *Atg16l1*^{VC} mice was again verified by blotting for lipidated LC3 (Fig. 2 G). We found that both WT and autophagy-deficient IEC rapidly responded to *H. hepaticus* infection, with comparable phosphorylation of Erk1/2 and NFκB p65 (Fig. 2 G). Furthermore, *Cxcl2* induction was also comparable between *Atg16l1*$^{fl/fl}$ and *Atg16l1*^{VC} IEC at 6h post *H. hepaticus* infection (Fig. 2 H).

Taken together, the *ex vivo* primary IEC stimulation experiments suggest that the exacerbated chemokine production observed in *Atg16l1*^{VC} mice during colitis (Fig. 2 A, B) is a consequence of the elevated inflammatory environment, rather than any intrinsic hyperactivity caused by autophagy impairment in IEC.

Several recent reports have linked the ER stress pathway and autophagy in the intestinal epithelium in the context of colitis (Adolph et al., 2013; Tschurtschenthaler et al., 2017). Therefore, we also assessed ER stress induction following iCM stimulation or *H. hepaticus* infection of primary IEC *ex vivo*. We found that *Grp78* expression was not altered following iCM stimulation in either

Atg16l1$^{fl/fl}$ or *Atg16l1*^{VC} IEC organoids (Fig. 2 I). In contrast, *H. hepaticus* infection of IEC monolayers resulted in comparably increased expression of *Grp78* in both *Atg16l1*$^{fl/fl}$ and *Atg16l1*^{VC} IEC (Fig. 2 J). Moreover, phosphorylation of eIF2α was also increased following *H. hepaticus* infection; and again the levels were similar in *Atg16l1*$^{fl/fl}$ or *Atg16l1*^{VC} IEC monolayers (Fig. 2 K). We also analyzed markers of ER stress in IEC isolated from *Atg16l1*$^{fl/fl}$ or *Atg16l1*^{VC} mice after colitis induction with *H. hepaticus* infection and αIL10R treatment. Consistent with the *in vitro* data, *Grp78* expression was elevated to similar levels during colitis in both *Atg16l1*$^{fl/fl}$ and *Atg16l1*^{VC} mice, both in isolated IEC fractions, as well as in whole colon tissue (Fig. 2 L, M).

Overall, these results suggest that, under these experimental conditions, ER stress pathways in IEC do not seem to be influenced by the presence or absence of the autophagy pathway.

Autophagy deficiency predisposes IEC to apoptosis

We next hypothesized that the absence of a functional autophagy pathway might predispose IEC to cell death during inflammatory conditions (Marino et al., 2014). To assess whether autophagy regulated apoptosis in IEC during chronic colitis, we assessed the number of apoptotic cells by TUNEL staining. We observed increased numbers of TUNEL-positive IEC in both caecal and colonic sections of *Atg16l1*^{VC} mice compared to *Atg16l1*$^{fl/fl}$ littermates at 2 weeks after colitis induction (Fig. 3 A). Moreover, western blot analyses of intestinal samples revealed increased levels of cleaved caspase 8 in isolated IEC lysates and whole colonic lysates obtained from *Atg16l1*^{VC} mice compared to those obtained from *Atg16l1*$^{fl/fl}$ littermates (Fig 3 B, C, D).

252 To determine whether the increased number of apoptotic IEC in *Atg16l1*^{VC} mice
253 was a consequence of the increased inflammation and elevated levels of pro-
254 inflammatory cytokines in *Atg16l1*^{VC} mice, or whether autophagy intrinsically
255 regulates apoptosis in IEC, we next assessed cytokine-induced apoptosis in
256 primary IEC *ex vivo*. Organoids generated from *Atg16l1*$^{fl/fl}$ and *Atg16l1*^{VC} mice
257 were stimulated with 40% iCM for 24h and cell death and apoptosis were
258 assessed in parallel. We observed that cell death and caspase 3/7 activity was
259 induced by iCM stimulation in both *Atg16l1*$^{fl/fl}$ and *Atg16l1*^{VC} IEC (Fig. 4 A, B),
260 with increased caspase activation detected in *Atg16l1*-deficient IEC (Fig. 4 B).
261 Furthermore, blockade of TNF and IFN-γ through addition of monoclonal
262 antibodies prevented cell death and apoptosis induction in IEC (Fig. 4 A, B),
263 suggesting that these cytokines were largely responsible for the apoptosis
264 induction in response to iCM. Indeed, stimulation of IEC organoids with TNF and
265 IFN-γ induced significantly higher levels of apoptosis (Fig. 4 A, B) and decreased
266 metabolic activity (Fig. 4 C, D) in *Atg16l1*^{VC} IEC organoids compared with
267 *Atg16l1*$^{fl/fl}$ organoids. Western blot analysis confirmed increased apoptosis levels
268 in the *Atg16l1*^{VC} IEC organoids after stimulation with TNF and IFN-γ, as they
269 showed increased cleavage of caspases 8 and 3 (Fig. 4 E) and staining for cleaved
270 caspase 3 revealed increased numbers of apoptotic cells and disrupted cell
271 morphology (Fig. 4 F).
272 To confirm that TNF induced elevated IEC apoptosis in *Atg16l1*^{VC} mice, we
273 assessed small intestinal epithelial cell apoptosis in mice that received an
274 intraperitoneal injection of TNF (Vereecke et al., 2014) (Fig. 5A). We observed
275 that *Atg16l1*^{VC} mice lost significantly more weight than littermate controls
276 following TNF injection (Fig5 B). Furthermore, TUNEL staining of small intestinal

277 tissue sections revealed increased numbers of apoptotic IEC in *Atg16l1*^{VC} mice
278 compared to *Atg16l1*$^{fl/fl}$ littermates (Fig. 5 C) and this correlated with increased
279 cleavage of caspase 8 in IEC lysates (Fig. 5 D,E).
280 Taken together, these results demonstrate that autophagy impairment renders
281 IEC more responsive to apoptosis induction following exposure to the pro-
282 inflammatory cytokine milieu present in the inflamed intestine.
283
284 ***TNF induced apoptosis drives exacerbated disease in Atg16l1^{VC} mice***
285 To functionally test whether TNF was the key driver of the increased IEC
286 apoptosis and exacerbated pathology in *Atg16l1*^{VC} mice in the complex setting of
287 chronic colitis, we induced colitis (*H. hepaticus* infection + anti-IL-10R
288 treatment) in *Atg16l1*^{VC} and *Atg16l1*$^{fl/fl}$ littermates and concomitantly treated a
289 group of mice with a blocking antibody against TNF (αTNF) (Fig. 6 A). We found
290 that, in contrast to their *Atg16l1*$^{fl/fl}$ littermates, *Atg16l1*^{VC} mice exhibited
291 significant weight loss during the first two weeks after colitis induction and that
292 this was completely prevented by treatment with αTNF (Fig. 6 B).
293 Furthermore, αTNF treatment also reduced intestinal pathology in *Atg16l1*^{VC}
294 mice (Fig. 6 C; Fig. S4 A, B, C). Finally, in these experiments we also assessed the
295 influence of αTNF treatment on apoptosis levels in IEC. We found that αTNF
296 treatment of *Atg16l1*^{VC} mice led to a marked reduction of TUNEL positive IEC
297 (Fig. 6 D; Fig. S4 D), as well as decreased levels of cleaved caspase 8 in IEC lysates
298 (Fig. 6 E-G). Indeed, αTNF treatment reduced the exacerbated apoptosis
299 induction in IEC of *Atg16l1*^{VC} mice during chronic colitis to the levels present in
300 IEC isolated from *Atg16l1*$^{fl/fl}$ littermates (Fig. 6 D-G). However, following TNF
301 blockade, some reduction of pathology was also observed in the *Atg16l1*$^{fl/fl}$ mice

and pro-inflammatory mediators were reduced in both *Atg16l1*$^{fl/fl}$ and *Atg16l1*^{VC} littermates at two weeks of colitis (Fig. 6 C; Fig. S4 A, B, C, E, F), suggesting several modes of action. In contrast, treating established colitis at day 6 post colitis induction with αTNF resulted in reduction of pathology only in the *Atg16l1*^{VC} mice (Fig. S5 A-C) and this correlated with reduced expression of pro-inflammatory mediators (Fig. S5 D, E).

Overall, these findings confirm that TNF-induced apoptosis of autophagy-deficient IEC is a key contributor to the exacerbated pathology, as blockade of the TNF pathway attenuates the disease.

Discussion

GWAS studies linked polymorphisms in *ATG16L1* and other autophagy genes to the development of IBD (Hampe et al., 2007; Rioux et al., 2007), suggesting an important role of autophagy in IBD pathogenesis. However, despite extensive investigation, the mechanistic relationship between autophagy and intestinal inflammation is not fully understood. We performed comparative analyses to assess the consequences of autophagy deficiency within different cellular compartments of the intestinal mucosa. We found that autophagy deficiency in LysM^{+} or CD11c^{+} cells only marginally affected chronic colitis development, whereas autophagy deficiency in IEC resulted in severely exacerbated pathology. This comparative approach, using tissue-specific *Atg16l1*-deficient mouse lines in the same disease model, highlights the pivotal role of autophagy in maintaining epithelial barrier function during inflammation.

Our results indicate that intestinal epithelial cells can function quite normally without autophagy, as long as intestinal homeostasis is not perturbed. We could not detect any abnormal growth pattern, differentiation or chemokine response of *Atg16l1*-deficient IEC, nor altered susceptibility during acute *Citrobacter rodentium* infection in *Atg16l1*^{VC} mice. *C. rodentium* infection induces an acute and self-limiting epithelial hyperplasia, accompanied by mild inflammation, both of which abate as the infection is cleared. In contrast, the *H. hepaticus* plus anti-IL-10R model results in sustained activation of innate and adaptive immune circuits that drive prolonged secretion of high concentrations of pro-inflammatory cytokines. Under the severe stress conditions present during this chronic colitis, *Atg16l1*-deficient IEC showed increased apoptosis, which contributed to exacerbation of intestinal inflammation.

The effects of autophagy-deficiency in IEC have been studied in several different models and mouse strains (Adolph et al., 2013; Benjamin et al., 2013; Cadwell et al., 2008; Conway et al., 2013; Tschurtschenthaler et al., 2017). It has been reported that autophagy deficiency in IEC resulted in enhanced bacterial translocation and inflammation following acute *Salmonella* challenge (Benjamin et al., 2013; Conway et al., 2013). However, when we evaluated *H. hepaticus* DNA levels in MLNs of mice in the chronic colitis model (data not shown) as well as systemic translocation of *C. rodentium* to liver and spleen following oral infection, we did not observe elevated levels in the *Atg16l1*^{VC} mice compared to *Atg16l1*$^{fl/fl}$ mice. These results suggest that epithelial autophagy may be important for containing invasive intestinal pathogens, but is not essential for preventing systemic dissemination of non-invasive pathogens.

Several studies reported altered granule structure in autophagy-deficient secretory IEC, such as Paneth cells and goblet cells (Adolph et al., 2013; Cadwell et al., 2008; Lassen et al., 2014; Patel et al., 2013). This phenotype was linked to increased pathology in norovirus infected *Atg16l1* hypomorphic mice during DSS colitis (Cadwell et al., 2010). However, whether aberrant Paneth cell morphology is a spontaneously occurring phenotype in autophagy-deficient IEC or requires an additional trigger such as viral or bacterial infection or ER stress is not clear (Adolph et al., 2013; Bel et al., 2017; Cadwell et al., 2008; Lassen et al., 2014; Patel et al., 2013). Furthermore, in IBD patients, altered granule structure in Paneth cells was associated with the *ATG16L1* T300A SNP (Cadwell et al., 2008). How this morphologic phenotype in the small intestine might predispose to colonic inflammation is poorly understood. Altered Paneth cell morphology could lead to altered AMP secretion, which might impact on microbiota

composition, a plausible factor for disease susceptibility. However it was recently described that *Atg16l1*^{VC} mice do not harbor an altered tissue-adherent microbiota in the ileum compared to *Atg16l1*$^{fl/fl}$ mice (Tschurtschenthaler et al., 2017). In our study, we used *Atg16l1*^{VC} and *Atg16l1*$^{fl/fl}$ littermates to avoid any potential microbiota effects and to ensure that any differences in disease susceptibility were due to genotype.

Several studies have illustrated compensatory mechanisms of ER stress and autophagy in intestinal epithelial cells. Indeed, transgenic mice lacking both the ER stress effector *Xbp1* and *Atg16l1* selectively in IEC develop severely exacerbated levels of ER stress and spontaneous pathology in the ileum (Adolph et al., 2013; Tschurtschenthaler et al., 2017). Furthermore, these investigators also reported spontaneous inflammation in the ileum of aged (>35weeks of age) *Atg16l1*^{VC} mice, concomitant with enhanced ER stress levels (Tschurtschenthaler et al., 2017). During chronic colitis induction we observed elevated levels of *Grp78* in colonic IEC, indicative of enhanced ER stress, however we detected similar levels of *Grp78* in IEC isolated from *Atg16l1*$^{fl/fl}$ and *Atg16l1*^{VC} mice, suggesting autophagy-independent regulation of ER stress during colonic inflammation. Moreover, *ex vivo* primary colonic IEC organoids stimulated with inflammatory cytokines or infected with *H. hepaticus* exhibited ER stress responses that were independent of the *Atg16l1* genotype. These findings suggest that autophagy and ER stress responses are only under certain conditions compensatory and could have different regulatory functions in the epithelium of the small intestine and colon.

Our study reveals a link between autophagy and apoptosis in IEC. We found that autophagy-deficiency in IEC enhanced apoptosis induction during inflammatory

conditions, thereby potentially weakening the barrier integrity. Furthermore, we observed that *Ag16l1*-deficient IEC organoids were hyper-susceptible to TNF-induced apoptosis. Similarly, during chronic colitis we observed that high intestinal TNF levels were associated with increased numbers of apoptotic IEC in *Atg16l1*^{VC} mice, but not *Atg16l1*$^{fl/fl}$ littermates. Of note, experimental administration of TNF also induced elevated levels of apoptosis in small intestinal epithelial cells of *Atg16l1*^{VC} mice, confirming an intrinsic control of IEC apoptosis by autophagy. Indeed blocking TNF during chronic colitis resulted in a specific and marked reduction of IEC apoptosis in *Atg16l1*^{VC} mice, confirming our hypothesis that the exacerbated pathology was caused by increased apoptosis of autophagy-deficient IEC under inflammatory conditions. However, continuous blockade of TNF throughout chronic colitis resulted in reduced pro-inflammatory chemokine levels and decreased intestinal pathology in both *Atg16l1*^{VC} and *Atg16l1*$^{fl/fl}$ mice, which indicates that TNF also has additional roles in chronic inflammation, such as immune cell activation and survival (Billmeier et al., 2016). Furthermore, although treatment of already established colitis with αTNF does not reduce pathology in WT (*Atg16l1*$^{fl/fl}$) mice (Kullberg et al., 2001; West et al., 2017), we found that it attenuated colitis in *Atg16l1*^{VC} mice, indicating that autophagy-deficiency in IEC renders the disease responsive towards αTNF treatment.

In accordance with our results, a recent study reported that autophagy-deficiency also renders small intestinal epithelial cells hyper susceptible to TNF-induced cell death (Matsuzawa-Ishimoto et al., 2017). These investigators used a model of intestinal inflammation triggered by infection with murine norovirus and treatment with DSS, and primarily focused on the small intestine, where a

lack of autophagy led to increased susceptibility to necroptosis and a loss of Paneth cells (Matsuzawa-Ishimoto et al., 2017). In contrast, we observed exacerbated activation of caspase-8 and caspase-3 in *Atg16l1*-deficient colonic IEC, as well as DNA fragmentation, all of which are hallmarks of apoptotic death. Therefore, although autophagy appears to generally protect IEC from TNF-induced cell death, there may be differences in the dominant death pathways triggered in distinct compartments or cell types (eg. small intestine versus colon; Paneth cells versus absorptive enterocytes), or during different types of inflammatory challenge (eg. Norovirus + DSS versus *H. hepaticus* + anti-IL-10R). These results are consistent with previous studies in which epithelial apoptosis has been linked to IBD pathology, with IEC having been described to be particularly susceptible to TNF induced apoptosis (Takahashi et al., 2014; Zeissig et al., 2004). For example, in a mouse model of spontaneous ileitis (SAMP1/YitFc model) a single shot of αTNF treatment ameliorated disease in the ileum correlating with reduction of epithelial apoptosis (Marini et al., 2003). Similarly, in the *Atg16l1*/*Xbp1*^{VC} model of spontaneous enteritis, the pathology scores strongly correlated with the degree of epithelial apoptosis (Adolph et al., 2013). Moreover, mice with hypomorphic expression of *Atg16l1* showed increased pathology with transmural inflammation in chemically induced colitis, which was reduced to wild-type levels by αTNF/ αIFNγ treatment (Cadwell et al., 2010). Together with these studies, our findings emphasise the links between autophagy in IEC and regulation of apoptosis in the inflamed intestine.

Of great interest is whether IBD patients bearing polymorphisms in autophagy genes present with increased IEC apoptosis and a more severe disruption of the

436 epithelial barrier. Although the IBD associated *ATG16L1* T300A SNP does not
437 confer loss off function under homeostatic conditions, it results in a
438 destabilization of the protein by enhancing caspase 3 dependent degradation
439 (Murthy et al., 2014). Therefore, under inflammatory conditions the T300A SNP
440 will enhance degradation of ATG16L1 and may thereby make the IEC more
441 susceptible to apoptosis. Interestingly, αTNF treatment of IBD patients has been
442 linked to reduction of IEC apoptosis (Zeissig et al., 2004), therefore a key future
443 issue is to determine whether patients that harbor genetic predisposition for IEC
444 apoptosis show better responsiveness to αTNF treatment. For example, it has
445 been shown that SNPs in *A20*, an inhibitory regulator of TNF signaling correlate
446 with αTNF responsiveness of patients (Vereecke et al., 2014). In this context, it is
447 striking that a recent study reported a correlation between the *ATG16L1* T300A
448 SNP and a beneficial outcome in colon cancer (Grimm et al., 2016), which might
449 be a result of increased apoptosis susceptibility of IEC harboring the SNP.
450 Overall our study proves that impaired autophagy in epithelial cells, but not in
451 myeloid cells, results in exacerbated chronic colonic inflammation. We showed
452 that autophagy-deficiency leads to enhanced cytokine-induced IEC apoptosis.
453 The potential to attenuate the exacerbated pathology in *Atg16l1*^{VC} mice by αTNF
454 treatment is of great clinical interest and may have implications for treatment of
455 IBD patients harboring SNPs in autophagy genes.

Acknowledgments

We thank members of the Kevin Maloy, Fiona Powrie and Katja Simon groups for helpful discussions and technical help. We are grateful to Gijs van den Brink for providing Noggin and R-spondin producing cell lines and technical help with the organoid cultures and to Herbert W Virgin and Thaddeus S Stappenbeck for mice with *lox*P-flanked *Atg16l1* alleles. We thank Michal Maj for assistance with the FACS analysis. Imaging was performed on Micron instruments funded by the Wellcome Trust Strategic Award (107457). J.P was supported by an EMBO longterm fellowship. K.J.M. and J.P. received funding from the MRC (MR/K011898/1 and MR/N02379X/1). K.J.M. received funding from the Wellcome Trust (102972). A.M.K. was supported by the Wellcome Trust Graduate Student Scholarship 097112.

Author Contributions

J.P. and A.M.K. designed and performed experiments. J.P. analyzed data. J.P. and K.J.M. secured funding and wrote the manuscript. A.M.K edited the manuscript.

Declaration of Interests

The authors declare no competing interests.

References

Adolph, T.E., Tomczak, M.F., Niederreiter, L., Ko, H.J., Bock, J., Martinez-Naves, E., Glickman, J.N., Tschurtschenthaler, M., Hartwig, J., Hosomi, S.*, et al.* (2013). Paneth cells as a site of origin for intestinal inflammation. Nature *503*, 272-276.

Bel, S., Pendse, M., Wang, Y., Li, Y., Ruhn, K.A., Hassell, B., Leal, T., Winter, S.E., Xavier, R.J., and Hooper, L.V. (2017). Paneth cells secrete lysozyme via secretory autophagy during bacterial infection of the intestine. Science *357*, 1047-1052.

Benjamin, J.L., Sumpter, R., Jr., Levine, B., and Hooper, L.V. (2013). Intestinal epithelial autophagy is essential for host defense against invasive bacteria. Cell host & microbe *13*, 723-734.

Billmeier, U., Dieterich, W., Neurath, M.F., and Atreya, R. (2016). Molecular mechanism of action of anti-tumor necrosis factor antibodies in inflammatory bowel diseases. World journal of gastroenterology *22*, 9300-9313.

Cadwell, K., Liu, J.Y., Brown, S.L., Miyoshi, H., Loh, J., Lennerz, J.K., Kishi, C., Kc, W., Carrero, J.A., Hunt, S.*, et al.* (2008). A key role for autophagy and the autophagy gene Atg16l1 in mouse and human intestinal Paneth cells. Nature *456*, 259-263.

Cadwell, K., Patel, K.K., Maloney, N.S., Liu, T.C., Ng, A.C., Storer, C.E., Head, R.D., Xavier, R., Stappenbeck, T.S., and Virgin, H.W. (2010). Virus-plus-susceptibility gene interaction determines Crohn's disease gene Atg16L1 phenotypes in intestine. Cell *141*, 1135-1145.

Chang, S., and Hanauer, S. (2017). Optimizing pharmacologic management of inflammatory bowel disease. Expert review of clinical pharmacology *10*, 595-607.

Cohen, B.L., and Sachar, D.B. (2017). Update on anti-tumor necrosis factor agents and other new drugs for inflammatory bowel disease. Bmj *357*, j2505.

Collins, J.W., Keeney, K.M., Crepin, V.F., Rathinam, V.A., Fitzgerald, K.A., Finlay, B.B., and Frankel, G. (2014). Citrobacter rodentium: infection, inflammation and the microbiota. Nature reviews Microbiology *12*, 612-623.

Conway, K.L., Kuballa, P., Song, J.H., Patel, K.K., Castoreno, A.B., Yilmaz, O.H., Jijon, H.B., Zhang, M., Aldrich, L.N., Villablanca, E.J.*, et al.* (2013). Atg16l1 is required for autophagy in intestinal epithelial cells and protection of mice from Salmonella infection. Gastroenterology *145*, 1347-1357.

de Souza, H.S.P., Fiocchi, C., and Iliopoulos, D. (2017). The IBD interactome: an integrated view of aetiology, pathogenesis and therapy. Nature reviews Gastroenterology & hepatology.

Grimm, W.A., Messer, J.S., Murphy, S.F., Nero, T., Lodolce, J.P., Weber, C.R., Logsdon, M.F., Bartulis, S., Sylvester, B.E., Springer, A.*, et al.* (2016). The Thr300Ala variant in ATG16L1 is associated with improved survival in human colorectal cancer and enhanced production of type I interferon. Gut *65*, 456-464.

Hampe, J., Franke, A., Rosenstiel, P., Till, A., Teuber, M., Huse, K., Albrecht, M., Mayr, G., De La Vega, F.M., Briggs, J.*, et al.* (2007). A genome-wide association scan of nonsynonymous SNPs identifies a susceptibility variant for Crohn disease in ATG16L1. Nature genetics *39*, 207-211.

519 Heijmans, J., van Lidth de Jeude, J.F., Koo, B.K., Rosekrans, S.L., Wielenga, M.C., van
520 de Wetering, M., Ferrante, M., Lee, A.S., Onderwater, J.J., Paton, J.C*., et al.* (2013).
521 ER stress causes rapid loss of intestinal epithelial stemness through activation of
522 the unfolded protein response. Cell reports *3*, 1128-1139.

523 Hendy, P., Hart, A., and Irving, P. (2016). Anti-TNF drug and antidrug antibody
524 level monitoring in IBD: a practical guide. Frontline gastroenterology *7*, 122-128.

525 Hue, S., Ahern, P., Buonocore, S., Kullberg, M.C., Cua, D.J., McKenzie, B.S., Powrie,
526 F., and Maloy, K.J. (2006). Interleukin-23 drives innate and T cell-mediated
527 intestinal inflammation. The Journal of experimental medicine *203*, 2473-2483.

528 Hwang, S., Maloney, N.S., Bruinsma, M.W., Goel, G., Duan, E., Zhang, L., Shrestha,
529 B., Diamond, M.S., Dani, A., Sosnovtsev, S.V*., et al.* (2012). Nondegradative role of
530 Atg5-Atg12/ Atg16L1 autophagy protein complex in antiviral activity of
531 interferon gamma. Cell host & microbe *11*, 397-409.

532 Jostins, L., Ripke, S., Weersma, R.K., Duerr, R.H., McGovern, D.P., Hui, K.Y., Lee, J.C.,
533 Schumm, L.P., Sharma, Y., Anderson, C.A*., et al.* (2012). Host-microbe interactions
534 have shaped the genetic architecture of inflammatory bowel disease. Nature *491*,
535 119-124.

536 Kabat, A.M., Harrison, O.J., Riffelmacher, T., Moghaddam, A.E., Pearson, C.F., Laing,
537 A., Abeler-Dorner, L., Forman, S.P., Grencis, R.K., Sattentau, Q*., et al.* (2016a). The
538 autophagy gene Atg16l1 differentially regulates Treg and TH2 cells to control
539 intestinal inflammation. eLife *5*.

540 Kabat, A.M., Pott, J., and Maloy, K.J. (2016b). The Mucosal Immune System and Its
541 Regulation by Autophagy. Frontiers in immunology *7*, 240.

542 Kullberg, M.C., Jankovic, D., Feng, C.G., Hue, S., Gorelick, P.L., McKenzie, B.S., Cua,
543 D.J., Powrie, F., Cheever, A.W., Maloy, K.J*., et al.* (2006). IL-23 plays a key role in
544 Helicobacter hepaticus-induced T cell-dependent colitis. The Journal of
545 experimental medicine *203*, 2485-2494.

546 Kullberg, M.C., Rothfuchs, A.G., Jankovic, D., Caspar, P., Wynn, T.A., Gorelick, P.L.,
547 Cheever, A.W., and Sher, A. (2001). Helicobacter hepaticus-induced colitis in
548 interleukin-10-deficient mice: cytokine requirements for the induction and
549 maintenance of intestinal inflammation. Infection and immunity *69*, 4232-4241.

550 Lassen, K.G., Kuballa, P., Conway, K.L., Patel, K.K., Becker, C.E., Peloquin, J.M.,
551 Villablanca, E.J., Norman, J.M., Liu, T.C., Heath, R.J*., et al.* (2014). Atg16L1 T300A
552 variant decreases selective autophagy resulting in altered cytokine signaling and
553 decreased antibacterial defense. Proceedings of the National Academy of
554 Sciences of the United States of America.

555 Liu, J.Z., van Sommeren, S., Huang, H., Ng, S.C., Alberts, R., Takahashi, A., Ripke, S.,
556 Lee, J.C., Jostins, L., Shah, T*., et al.* (2015). Association analyses identify 38
557 susceptibility loci for inflammatory bowel disease and highlight shared genetic
558 risk across populations. Nature genetics *47*, 979-986.

559 Lonnfors, S., Vermeire, S., Greco, M., Hommes, D., Bell, C., and Avedano, L. (2014).
560 IBD and health-related quality of life -- discovering the true impact. Journal of
561 Crohn's & colitis *8*, 1281-1286.

562 Maloy, K.J., and Powrie, F. (2011). Intestinal homeostasis and its breakdown in
563 inflammatory bowel disease. Nature *474*, 298-306.

564 Maloy, K.J., Salaun, L., Cahill, R., Dougan, G., Saunders, N.J., and Powrie, F. (2003).
565 CD4+CD25+ T(R) cells suppress innate immune pathology through cytokine-
566 dependent mechanisms. The Journal of experimental medicine *197*, 111-119.

567 Marini, M., Bamias, G., Rivera-Nieves, J., Moskaluk, C.A., Hoang, S.B., Ross, W.G.,
568 Pizarro, T.T., and Cominelli, F. (2003). TNF-alpha neutralization ameliorates the
569 severity of murine Crohn's-like ileitis by abrogation of intestinal epithelial cell
570 apoptosis. Proceedings of the National Academy of Sciences of the United States
571 of America *100*, 8366-8371.

572 Marino, G., Niso-Santano, M., Baehrecke, E.H., and Kroemer, G. (2014). Self-
573 consumption: the interplay of autophagy and apoptosis. Nature reviews
574 Molecular cell biology *15*, 81-94.

575 Matsuzawa-Ishimoto, Y., Shono, Y., Gomez, L.E., Hubbard-Lucey, V.M., Cammer,
576 M., Neil, J., Dewan, M.Z., Lieberman, S.R., Lazrak, A., Marinis, J.M.*, et al.* (2017).
577 Autophagy protein ATG16L1 prevents necroptosis in the intestinal epithelium.
578 The Journal of experimental medicine *214*, 3687-3705.

579 Mizushima, N., Yoshimori, T., and Ohsumi, Y. (2011). The role of Atg proteins in
580 autophagosome formation. Annual review of cell and developmental biology *27*,
581 107-132.

582 Moon, C., Vandussen, K.L., Miyoshi, H., and Stappenbeck, T.S. (2013).
583 Development of a primary mouse intestinal epithelial cell monolayer culture
584 system to evaluate factors that modulate IgA transcytosis. Mucosal immunology.

585 Murthy, A., Li, Y., Peng, I., Reichelt, M., Katakam, A.K., Noubade, R., Roose-Girma,
586 M., Devoss, J., Diehl, L., Graham, R.R.*, et al.* (2014). A Crohn's disease variant in
587 Atg16l1 enhances its degradation by caspase 3. Nature.

588 Neurath, M.F. (2014). Cytokines in inflammatory bowel disease. Nature reviews
589 Immunology *14*, 329-342.

590 Patel, K.K., Miyoshi, H., Beatty, W.L., Head, R.D., Malvin, N.P., Cadwell, K., Guan,
591 J.L., Saitoh, T., Akira, S., Seglen, P.O.*, et al.* (2013). Autophagy proteins control
592 goblet cell function by potentiating reactive oxygen species production. The
593 EMBO journal *32*, 3130-3144.

594 Pfaffl, M.W. (2001). A new mathematical model for relative quantification in real-
595 time RT-PCR. Nucleic acids research *29*, e45.

596 Rioux, J.D., Xavier, R.J., Taylor, K.D., Silverberg, M.S., Goyette, P., Huett, A., Green,
597 T., Kuballa, P., Barmada, M.M., Datta, L.W.*, et al.* (2007). Genome-wide association
598 study identifies new susceptibility loci for Crohn disease and implicates
599 autophagy in disease pathogenesis. Nature genetics *39*, 596-604.

600 Saitoh, T., Fujita, N., Jang, M.H., Uematsu, S., Yang, B.G., Satoh, T., Omori, H., Noda,
601 T., Yamamoto, N., Komatsu, M.*, et al.* (2008). Loss of the autophagy protein
602 Atg16L1 enhances endotoxin-induced IL-1beta production. Nature *456*, 264-268.

603 Schiering, C., Krausgruber, T., Chomka, A., Frohlich, A., Adelmann, K., Wohlfert,
604 E.A., Pott, J., Griseri, T., Bollrath, J., Hegazy, A.N.*, et al.* (2014). The alarmin IL-33
605 promotes regulatory T-cell function in the intestine. Nature *513*, 564-568.

606 Song-Zhao, G.X., and Maloy, K.J. (2014). Experimental mouse models of T cell-
607 dependent inflammatory bowel disease. Methods in molecular biology *1193*,
608 199-211.

609 Song-Zhao, G.X., Srinivasan, N., Pott, J., Baban, D., Frankel, G., and Maloy, K.J.
610 (2014). Nlrp3 activation in the intestinal epithelium protects against a mucosal
611 pathogen. Mucosal immunology *7*, 763-774.

612 Takahashi, N., Vereecke, L., Bertrand, M.J., Duprez, L., Berger, S.B., Divert, T.,
613 Goncalves, A., Sze, M., Gilbert, B., Kourula, S.*, et al.* (2014). RIPK1 ensures
614 intestinal homeostasis by protecting the epithelium against apoptosis. Nature
615 *513*, 95-99.

616 Thurston, T.L., Wandel, M.P., von Muhlinen, N., Foeglein, A., and Randow, F.
617 (2012). Galectin 8 targets damaged vesicles for autophagy to defend cells against
618 bacterial invasion. Nature *482*, 414-418.

619 Tschurtschenthaler, M., Adolph, T.E., Ashcroft, J.W., Niederreiter, L., Bharti, R.,
620 Saveljeva, S., Bhattacharyya, J., Flak, M.B., Shih, D.Q., Fuhler, G.M.*, et al.* (2017).
621 Defective ATG16L1-mediated removal of IRE1alpha drives Crohn's disease-like
622 ileitis. The Journal of experimental medicine.

623 Uhlig, H.H., Coombes, J., Mottet, C., Izcue, A., Thompson, C., Fanger, A., Tannapfel,
624 A., Fontenot, J.D., Ramsdell, F., and Powrie, F. (2006). Characterization of
625 Foxp3+CD4+CD25+ and IL-10-secreting CD4+CD25+ T cells during cure of
626 colitis. Journal of immunology *177*, 5852-5860.

627 Vereecke, L., Vieira-Silva, S., Billiet, T., van Es, J.H., Mc Guire, C., Slowicka, K., Sze,
628 M., van den Born, M., De Hertogh, G., Clevers, H.*, et al.* (2014). A20 controls
629 intestinal homeostasis through cell-specific activities. Nature communications *5*,
630 5103.

631 Ward, J.M., Fox, J.G., Anver, M.R., Haines, D.C., George, C.V., Collins, M.J., Jr.,
632 Gorelick, P.L., Nagashima, K., Gonda, M.A., Gilden, R.V.*, et al.* (1994). Chronic
633 active hepatitis and associated liver tumors in mice caused by a persistent
634 bacterial infection with a novel Helicobacter species. Journal of the National
635 Cancer Institute *86*, 1222-1227.

636 Wei, J., Long, L., Yang, K., Guy, C., Shrestha, S., Chen, Z., Wu, C., Vogel, P., Neale, G.,
637 Green, D.R.*, et al.* (2016). Autophagy enforces functional integrity of regulatory T
638 cells by coupling environmental cues and metabolic homeostasis. Nature
639 immunology *17*, 277-285.

640 West, N.R., Hegazy, A.N., Owens, B.M.J., Bullers, S.J., Linggi, B., Buonocore, S.,
641 Coccia, M., Gortz, D., This, S., Stockenhuber, K.*, et al.* (2017). Oncostatin M drives
642 intestinal inflammation and predicts response to tumor necrosis factor-
643 neutralizing therapy in patients with inflammatory bowel disease. Nature
644 medicine *23*, 579-589.

645 Zeissig, S., Bojarski, C., Buergel, N., Mankertz, J., Zeitz, M., Fromm, M., and
646 Schulzke, J.D. (2004). Downregulation of epithelial apoptosis and barrier repair
647 in active Crohn's disease by tumour necrosis factor alpha antibody treatment.
648 Gut *53*, 1295-1302.

649 Zhang, H., Zheng, L., McGovern, D.P., Hamill, A.M., Ichikawa, R., Kanazawa, Y., Luu,
650 J., Kumagai, K., Cilluffo, M., Fukata, M., *et al.* (2017). Myeloid ATG16L1 Facilitates
651 Host-Bacteria Interactions in Maintaining Intestinal Homeostasis. Journal of
652 immunology *198*, 2133-2146.
653
654

Figure legend

Figure 1: Epithelial autophagy dampens chronic colitis

Atg16l1^{VC}, *Atg16l1*^{CD11c}, *Atg16l1*^{LysM} or *Atg16l1*$^{fl/fl}$ littermates were orally infected with 10^8 CFU *H.h*. on 3 consecutive days and injected with 1 mg anti-IL10R weekly. **A)** Schematic of treatment protocol. **B, C**) Histopathology of the caecum (B) or colon (C) was assessed on day 14 and presented relative to the respective *Atg16l1*$^{fl/fl}$ littermates. **D, E**) Representative H&E sections of caecum (D) or colon (E) from *Atg16l1*^{VC} or *Atg16l1*$^{fl/fl}$ littermates at day 14. **F, G)** Histopathology scores of the caecum (F) and colon (G) of *Atg16l1*^{VC} and *Atg16l1*$^{fl/fl}$ littermates at 2 and 4 weeks. **H)** Weight curves of *Atg16l1*^{VC} and *Atg16l1*$^{fl/fl}$ littermates during chronic colitis. **I)** Total numbers of $CD4^+TCR\beta^+$ T cells in isolated colonic LPLs from *Atg16l1*^{VC} and *Atg16l1*$^{fl/fl}$ littermates at steady-state and at day 14 after colitis induction. **J-L)** TNF (J), IFNγ (K) and IL-1β (L) levels in colonic organ culture supernatants from *Atg16l1*^{VC} and *Atg16l1*$^{fl/fl}$ littermates at steady-state and at day 14 after colitis induction.

Data are combined from at least 3 independent experiments (B,C,F,G,H,I) (representative D,E) or 2 independent experiments (J,K,L). Each dot represents an individual mouse (B,C,F,G,I,J,K,L), or data are shown as mean ± s.e.m (H). Horizontal bars denote medians. Scale bars are 100 μm. Statistical significance was determined using Kruskal-Wallis test with correction for multiple comparisons (B, C), two-way analysis of variance (ANOVA) with Bonferroni's correction for multiple comparisons (H) or Mann Whitney test, * $p<0.05$; ** $p<0.01$; *** $p<0.001$. ns – not significant, *H.h*. – *Helicobacter hepaticus*, p.i. – post infection.

Figure 2: *Atg16l1*-deficient IEC do not exhibit enhanced inflammatory or stress responses

A, B) qPCR analysis of *Cxcl2* (A) and *Cxcl5* (B) expression in IEC isolated from *Atg16l1*^{VC} and *Atg16l1*$^{fl/fl}$ littermates at day 14 after colitis induction. **C-K)** IEC from *Atg16l1*^{VC} and *Atg16l1*$^{fl/fl}$ mice were grown *ex vivo* in organoids. Inflammatory conditioned medium (iCM) was harvested from LPL cultures from colitic mice. **C)** Organoids stimulated with 10% iCM for 30 min were stained for pSTAT3 (red) and STAT3 (green) and DAPI (blue). **D)** *Atg16l1*^{VC} and *Atg16l1*$^{fl/fl}$ organoids were stimulated with 10% iCM for indicated times and lysates were probed with antibodies directed against indicated proteins. **E, F)** qPCR analysis of *Cxcl2* (E) and *Cxcl5* (F) expression by *Atg16l1*^{VC} and *Atg16l1*$^{fl/fl}$ organoids treated with 10% iCM for 6h. **G, H)** Monolayers of *Atg16l1*^{VC} and *Atg16l1*$^{fl/fl}$ IEC were infected with *H.h.* at a MOI of 100:1. **G)** Lysates were blotted after indicated times for indicated proteins. **H)** qPCR analysis of *Cxcl2* expression by IEC monolayers after 6h of *H.h*. infection. **I)** qPCR analysis of *Grp78* expression by *Atg16l1*^{VC} and *Atg16l1*$^{fl/fl}$ organoids treated with 10% iCM for 12h. **J)** qPCR analysis of *Grp78* expression by *Atg16l1*^{VC} and *Atg16l1*$^{fl/fl}$ monolayers infected with *H.h*. (MOI 100:1) for 6h. **K)** Lysates of *Atg16l1*^{VC} and *Atg16l1*$^{fl/fl}$ monolayers infected with *H.h*. (MOI 100:1) were blotted after indicated times for peIF2a and eIF2a. **L, M)** qPCR analysis of *Grp78* expression in whole colonic tissue (L) or IEC (M) isolated from *Atg16l1*^{VC} and *Atg16l1*$^{fl/fl}$ littermates at day 14 after colitis induction.

Data are representative of 2 (C, G, K) or 3 (A, B, D, L, M) independent experiments or combined from at least 3 independent experiments (E, F, H, I, J).

Data are shown as medians ± s.e.m (E, F, H, I, J), or each dot represents individual mouse (A, B, L, M). Horizontal bars denote medians. Scale bar is 50 μm. Statistical significance was determined using Mann Whitney test, * $p<0.05$; ** $p<0.01$; *** $p<0.001$. iCM – inflammatory conditioned medium, *H.h*. – *Helicobacter hepaticus*.

Figure 3: Autophagy deficiency increases IEC apoptosis during chronic colitis

Atg16l1^{VC} and *Atg16l1*$^{fl/fl}$ littermates were orally infected with 10^8 CFU *H.h*. on 3 consecutive days and injected with 1 mg anti-IL10R weekly. **A)** TUNEL (red) stainings of caecum and mid colon sections isolated at day 14 after colitis induction. Counterstaining with wheat germ agglutinin (green) and DAPI (blue). **B,C)** Lysates of IEC isolated from *Atg16l1*^{VC} and *Atg16l1*$^{fl/fl}$ littermates at 1 week (B) and 2 weeks (C) after colitis induction were blotted for cleaved caspase 8. **D)** Quantification of western blot bands of caspase 8 p43 (upper panel) and p18 (lower panel) in lysates of whole colon tissue isolated from *Atg16l1*^{VC} and *Atg16l1*$^{fl/fl}$ littermates at day 14 after colitis induction.

Data are representative of 3 independent experiments (A-D). Each dot represents individual band (D). Horizontal bars denote median. Scale bar is 100 μm. ctl- control, Atg- *Atg16l1*, *H.h*. – *Helicobacter hepaticus*.

Figure 4: Autophagy deficiency predisposes IEC to apoptosis

Atg16l1^{VC} and *Atg16l1*$^{fl/fl}$ IEC were grown *ex vivo* in organoids. Inflammatory conditioned medium (iCM) was harvested from LPL cultures from colitic mice. **A, B)** *Atg16l1*^{VC} and *Atg16l1*$^{fl/fl}$ organoids were stimulated for 18h with 40% iCM (iCM); iCM plus anti-TNF (10μg/ml) and anti-IFNγ (10μg/ml) (iCM+αα); or with TNF (100ng/ml) and IFNγ (20ng/ml) (IFNγ + TNF). Cytotoxicity (A) and apoptosis (B) were assessed with Apotox-Glo (Promega kit). **C, D)** *Atg16l1*^{VC} and *Atg16l1*$^{fl/fl}$ IEC organoids were stimulated with TNF (100ng/ml) and IFNγ (20ng/ml) for 24h prior to incubation with alamarBlue for 3h. C) Fluorescence intensity was measured at 540nm/ 590nm, normalized to values prior to treatment and plotted relative to the untreated genotype control. D) Picture of the 96-well plate after further 24h incubation with alamarBlue. **E)** *Atg16l1*^{VC} and *Atg16l1*$^{fl/fl}$ IEC organoids were stimulated with TNF (100ng/ml) and IFNγ (20ng/ml) for indicated times and caspase 8 and 3 cleavage detected by western blot. **F)** *Atg16l1*^{VC} and *Atg16l1*$^{fl/fl}$ IEC organoids were stimulated with TNF (100ng/ml) and IFNγ (20ng/ml) for 18h and cells were stained for cleaved caspase 3 (red), the epithelial marker E-cadherin (green) and DAPI (blue).

Data are representative of 3 independent experiments (A-F). Data are shown as mean ± s.e.m (A-C). Scale bar is 50 μm. Statistical significance was determined using students t test, * $p<0.05$; ** $p<0.01$; *** $p<0.001$. iCM – inflammatory conditioned medium, αα – anti-TNF and anti-IFNγ, T – TNF, γ - IFNγ.

Figure 5: TNF induces epithelial apoptosis in *Atg16l1*^{VC} mice

Atg16l1^{VC} and *Atg16l1*$^{fl/fl}$ littermates were injected intraperitoneally with 10 µg of TNF and sacrificed 6h later. **A)** Schematic of the treatment protocol. **B)** Body weight at 6h post-injection as percentage of initial weight. **C)** TUNEL staining (red) of small intestinal sections; counterstaining with wheat germ agglutinin (green) and DAPI (blue). **D, E)** Representative western blot (D) and quantification (E) of cleaved caspase 8 in isolated IEC.

Data are combined (B, E) or representative (C, D) of 3 independent experiments. Each dot represents individual mouse (B, E). Scale bar is 100 µm. Statistical significance was determined using Mann Whitney test, * $p<0.05$; ** $p<0.01$. Horizontal bars denote medians. i.p.- intraperitoneal, WGA – wheat germ agglutinin, cl. casp8- cleaved caspase 8, ctl- control, Atg - Atg16l1.

Figure 6: TNF blockade attenuates colitis and IEC apoptosis in *Atg16l1*^{VC} mice

Atg16l1^{VC} and *Atg16l1*$^{fl/fl}$ littermates were orally infected with 10^8 CFU *H.h*. on 3 consecutive days and injected with 1 mg anti-IL10R i.p., with some cohorts also receiving 1 mg anti-TNF i.p. at d0 and d6. **A)** Schematic of the treatment protocol. **B)** Weight curves and **C)** representative micrographs of H&E stained colonic sections from *Atg16l1*^{VC} and *Atg16l1*$^{fl/fl}$ littermates at day 14 after colitis induction. **D)** Representative images of TUNEL (red) staining of caecal sections at day 14 after colitis induction; counterstaining with WGA (green) and DAPI (blue). **E, F, G)** Western blot analysis for cleaved caspase 8 in colonic IEC lysates isolated from *Atg16l1*^{VC} and *Atg16l1*$^{fl/fl}$ littermates at day 14 after colitis induction. Representative blot (E) and quantification of caspase 8 p43 (F) and p18 (G) relative to tubulin.

Data are combined (B, F, G) or representative (C, D, E) from 3 independent experiments. Each dot represents an individual mouse (F, G), or data are shown as mean ± s.e.m (B). Scale bars are 100 μm. Statistical significance was determined using two-way analysis of variance (ANOVA) with Bonferroni's correction for multiple comparisons. Results shown for comparison between *Atg16l1*^{VC} and *Atg16l1*^{VC} + αTNF group (B) or Mann Whitney test, ** $p<0.01$; *** $p<0.001$, **** $p<0.0001$. *H.h.* – *Helicobacter hepaticus*, pi – post infection.

STAR Methods

Contact for Reagent and Resource Sharing

Further information and requests for resources and reagents should be directed to and will be fulfilled by the Lead Contact, Dr. Kevin Maloy (kevin.maloy@path.ox.ac.uk).

Experimental model and subject details

Mice

Atg16l1$^{fl/fl}$ mice and *Atg16l1*$^{fl/fl}$ Villin-Cre (*Atg16l1*^{VC}) mice were generated and provided by the H. Virgin laboratory (Washington University, Saint Louis, MO, USA), as described (Hwang et al., 2012). *Atg16l1*$^{fl/fl}$ mice were crossed to C57BL/6J-Tg (Itgax-cre,-EGFP) and *Lyz2*$^{tm1(cre)}$ to generate *Atg16l1*^{CD11c} and *Atg16l1*^{LysM} mice. All above strains were bred and maintained under specific pathogen-free conditions and tested negative for *Helicobacter* species. Mice were housed in groups of 2-5 in individually ventilated cages (IVC) and were 6-12 weeks old when used. All procedures on mice were conducted in accredited animal facilities at the University of Oxford (Oxford, UK) in accordance with the UK Scientific Procedures Act (1986) under a project license (PPL 30/3423) authorized by the UK Home Office Animal Procedures Committee and approved by the local ethical review panel. Mice were bred hemizygous for the Cre allele, resulting in *Atg16l1*$^{fl/fl}$ Cre^{-} and *Atg16l1*$^{fl/fl}$ Cre^{+} littermates. The colitis models show some variability over time and between cages, which suggest a strong contribution by the microbiota. Therefore, in all experiments age- and sex-matched littermates were used that were kept co-housed throughout the experiments. Mice were allocated to experimental groups according to genotype,

litter and cage, ensuring that in every cage and from every litter both genotypes were present and treatment regimes were evenly distributed over cages.

Organoid culture

Organoids were cultured as previously described by van den Brink and colleagues (Heijmans et al., 2013). Colonic crypts were isolated from *Atg16l1*$^{fl/fl}$ mice or *Atg16l1*^{VC} mice and seeded in matrigel (Corning, Wiesbaden, Germany) and cultured in the presence of N2 and B27 supplements (Fisher Scientific- UK Ltd, Loughborough, UK), mEGF (Fisher Scientific; 50ng/ml), Y-27632 (Sigma-Aldrich, St. Louis, US; 10uM), N-Acetylcysteine (Sigma-Aldrich, 1mM) and conditioned medium containing Wnt3a (20%), Noggin (20%) and R-Spondin (10%). The conditioned media were generated from Rspol-Fc Hek 293T cells (kind gift from Dr. Calvin Kuo, Stanford) and Nog-Fc Hek 293T cells (kind gift from Dr. Gjis van den Brink, Amsterdam) and Wnt3A L cells (ATCC® CRL-2647™). After expansion by several passages organoids were seeded in 24 well plates for experiments with indicated stimuli.

For bacterial infection experiments, organoids were trypsinized, filtered and about 4 wells (from a 24-well plate) of organoids were seeded into one collagen-coated 24-well plate well (Collagen-I, A1048301, ThermoFisher Scientific). The resulting IEC monolayers were cultured in complete organoid medium for 2 days prior to infection.

Method details

Colitis models

H. hepaticus (NCI-Frederick isolate 1A) (Ward et al., 1994) was cultured in TSB media supplemented with 10% FCS and trimethoprim (5μg/ml), vancomycin (10 μg/ml) and polymyxin B (25 IU/ml) (TVP, Oxoid) under microaerophilic conditions (10% CO_2, 10% H_2, 80% N_2) (Song-Zhao and Maloy, 2014). Chronic colitis was induced by infecting mice intragastrically with 10^8 CFU *H. hepaticus* at 3 consecutive days and injecting intraperitoneally 1 mg of mAb anti-IL10R (clone 1B1.2) weekly. For protection experiments mice were treated with 1 mg of mAb anti-TNF (XT3.11) weekly.

For infection experiments *C. rodentium* (ICC169) was grown in Luria Broth supplemented with nalidixic acid in log phase to an OD of 1. Mice were infected intragastrically with $5x10^9$ CFU *C. rodentium* (Song-Zhao et al., 2014).

TNF-induced enteropathy

Mice were injected intraperitoneally with 10 μg of murine TNF (Peprotech) and scarified after 6h for tissue isolation.

Histological assessment of intestinal inflammation

Mice were sacrificed at indicated time points whereupon tissue sections were fixed in buffered 10% formalin and paraffin-embedded. Histological analysis of H&E stained sections for intestinal inflammation was performed as described (Song-Zhao and Maloy, 2014). Briefly, inflammation was graded semi-quantitatively on a scale from 0 to 3, for four criteria; (a) epithelial hyperplasia and goblet cell depletion, (b) lamina propria leukocyte infiltration, (c) area of

855 tissue affected, and (d) markers of severe inflammation, including crypt
856 abscesses, sub- mucosal inflammation, and ulceration. Scores for individual
857 criteria were added up for an overall inflammation score between 0 and 12.
858 Scoring was performed by two scientists in a blinded fashion.
859
860 ***Isolation of cells and flow cytometry analysis and sorting***
861 For IEC preparations colons were isolated and digested in 5mM EDTA in RPMI
862 (5% FCS) for 10 min. Digests were vigorously shaken and cell suspension
863 filtered. Cell pellets were lysed in RLT (Qiagen, Manchester, UK) for RNA
864 preparation or RIPA buffer containing proteinase inhibitors (Roche) for western
865 blot analysis. Cell suspensions from spleen, mLN, and intestinal lamina propria
866 were prepared as previously described (Uhlig et al., 2006). For intracellular
867 cytokine staining cells were stimulated for 3h with PMA (100 ng/ml) and
868 Ionomycin (1 μg/ml) in the presence of Brefeldin A (10 μg/ml). For FACS
869 analysis the following antibodies from eBioscience (Hatfield, UK) were used:
870 anti-CD4 (GK1.5), anti-TCRβ (H57-597), anti-CD45 (30-F11), anti-GR.1 (RB6-
871 8C5), anti-Foxp3 (FJK-16s), anti-IFN-γ (XMG1.2), anti-IL-17A (eBio17B7). The
872 following antibodies were from BioLegend (San Diego, USA): anti-F4/80 (BMB),
873 anti-CD11b (M1/70). Fixable Viability Dye from eBioscience was used to stain
874 dead cells. For data acquisition a Cyan ADP was used (Beckman Coulter, High
875 Wycombe, UK) and analyzed using FlowJo software (Tree Star, Ashland, USA). To
876 verify excision efficiency of Atg16l1 in distinct cellular population of the
877 intestinal mucosa, cells were sorted with a MoFlo Astrios Sorter (Beckman
878 Coulter). LPL were stained with viability dye (eFluor 780), anti-CD45-APC, anti-
879 CD11c-Fitc, anti-MHC2-eFluor450, anti-CD11b-PerCP Cy5.5, anti-CD64-PE and

two populations were collected in RLT buffer: DC defined as live, $CD45^+$, $CD11c^+$ and $MHC2^+$ and macrophages as live, $CD45^+$, $CD11b^+$ and $CD64^+$.

Immunofluorescent stainings

Colonic tissue samples were formalin-fixed and paraffin-embedded. Sections were deparaffinized, rehydrated, proteinase k treated and stained according to the *in situ* cell death detection kit, Fluorescein (Sigma-Aldrich). Counterstaining was performed with Wheat Germ Agglutinin, Alexa Fluor 647 Conjugate (Fisher Scientific) and DAPI (Sigma-Aldrich). Slides were mounted with ProLong Gold Antifade Mountant (Fisher Scientific).

For immunofluorescent staining of organoids, cells were grown on cover slips. Following stimulation cells were fixed with 4% paraformaldehyde at room temperature followed by methanol treatment at -20C. Cells were blocked in 5% goat serum, 5% BSA and 0.5% saponine. Stainings were performed with pAb mouse-anti-Ecadherin (BD Bioscience), rabbit-anti-phospho Stat 3, mouse-anti Stat 3 and rabbit-anti-cleaved caspase 3 from Cell Signalling (Danvers, USA) and goat-anti-rabbit Alexa Fluor 555 or goat-anti-mouse Alexa Fluor 488 (Fisher Scientific). Images were acquired with an Olympus Fluoview FV1000 confocal microscope and Olympus Fluoview Software (Olympus, Tokyo, Japan). One representative image of the TUNEL stained sections per mouse was taken after careful screening of all sections while blinded for the genotype. We then grouped the images according to the treatment/ genotype and a different still blinded scientist in terms of genotype or treatment chose the representative image per group.

Western blot analysis

For immunoblot analysis cells were lysed after indicated times in RIPA buffer and 1-5 ug total protein were analyzed per lane. For detection the following primary antibodies were used: anti-LC3 antibody (L7543; Sigma-Aldrich) anti-phospho-Stat3, anti-Stat3, anti-phospho-ERK1/2, anti-phospho-Mek, anti-phospho-p65, anti-p65, anti-phospho-eIF2a, anti-eIF2a, anti-phospho-p38, anti-cleaved caspase 8, anti-cleaved caspase 3, (all antibodies from Cell Signalling) and anti-tubulin antibody (sc5286, Santa Cruz Biotechnology, Dallas, USA), and secondary HRP conjugated anti–rabbit or anti-mouse antibody (Cell Signalling).

Cell death and metabolic assay

For cell death detection the ApoTox Glo Assay from Promega (Southampton, UK) was used. Organoids were seeded in 4ul matrigel in a 96 well pate; following stimulation the ApoTox Glo Assay was used according to manufactures instructions.

For the assessment of metabolic activity with AlamarBlue (Fisher Scientific) as a correlate of cell viability organoids were seeded in 4ul matrigel in a 96 well plate. Organoids were incubated with AlamarBlue for 3h prior to stimulation to generate reference metabolic activity. Fluorescent intensity was measured at 540nm/ 590nm. Following stimulation same procedure was repeated and values were normalized to untreated values.

RNA and qPCR

For qPCR analysis cells were lysed in RLT and RNA purified using the RNeasy kit from Qiagen. 1-2 μg of RNA were reverse transcribed with SuperScript III

reverse transcriptase (Fisher Scientific) and quantitative real-time PCR was carried out with the StepOnePlus Real time system from Applied Biosystems. RNA from sorted cell populations was purified with the RNeasy Micro kit (Qiagen) and all RNA was transcribed. qPCR Mastermix (Eurogentec, Liege, Belgium) was used for Taqman reactions and iQ Sybr Green Supermix (Biorad, Kidlington, UK) for Sybr green reactions. Taqman probes for *Cxcl2* (Mm_00436450_m1), *Atg16l1* (Mm_00513084_m1) and *Hprt* (Mm_03024075_m1) were from Applied Biossystems and primers for *Grp78* (forwards: acttggggaccacctattcct; reverse: atcgccaatcagacgctcc) for Sybr green PCR from Sigma-Aldrich. Relative expression was analysed according to the Pfaffl method (Pfaffl, 2001).

Organ explants

Pieces of 10-20 mg of colon or caecum were isolated and cultured in complete RPMI (10% FCS, 5µM β-mercaptoethanol (Fisher Scientific), 1x Penicillin/Streptomycin (Fisher Scientific), 1x Glutamine (Fisher Scientific)) for 20h. Supernatants were tested for cytokine levels with the Luminex Multiplex Assay (Thermo Fisher Scientific) and normalised to input tissue weight.

Generation of inflammatory conditioned medium (iCM)

Lamina propria leukocytes were isolated from C57Bl/6 mice at 2 weeks of *H.h.* + αIL10R colitis and $2.3x10^6$ cell/ml were seeded in complete RPMI for 20h. Supernatants from cells of 7 mice were pooled and frozen at -80C.

Quantification and statistical analysis

For weight curves p-values were determined by two-way ANOVA with Bonferroni post-tests. For other experiments, p-values were determined by nonparametric Mann–Whitney test, or by Kruskal-Wallis test with correction for multiple comparisons. Differences were considered statistically significant when $p < 0.05$ (* $p< 0.05$, ** $p< 0.01$, *** $p< 0.001$). Statistics were calculated using GraphPad Prism 6 software. The statistical tests applied, definition of center, dispersion and precision measures depicted, as well as the number of experimental repeats are specified in the figure legends.

For *in vivo* experiments, sample size was determined by power analysis using power of trial software, which calculates a power value based on X^2 test statistics. Calculated required sample sizes were applied whenever possible.

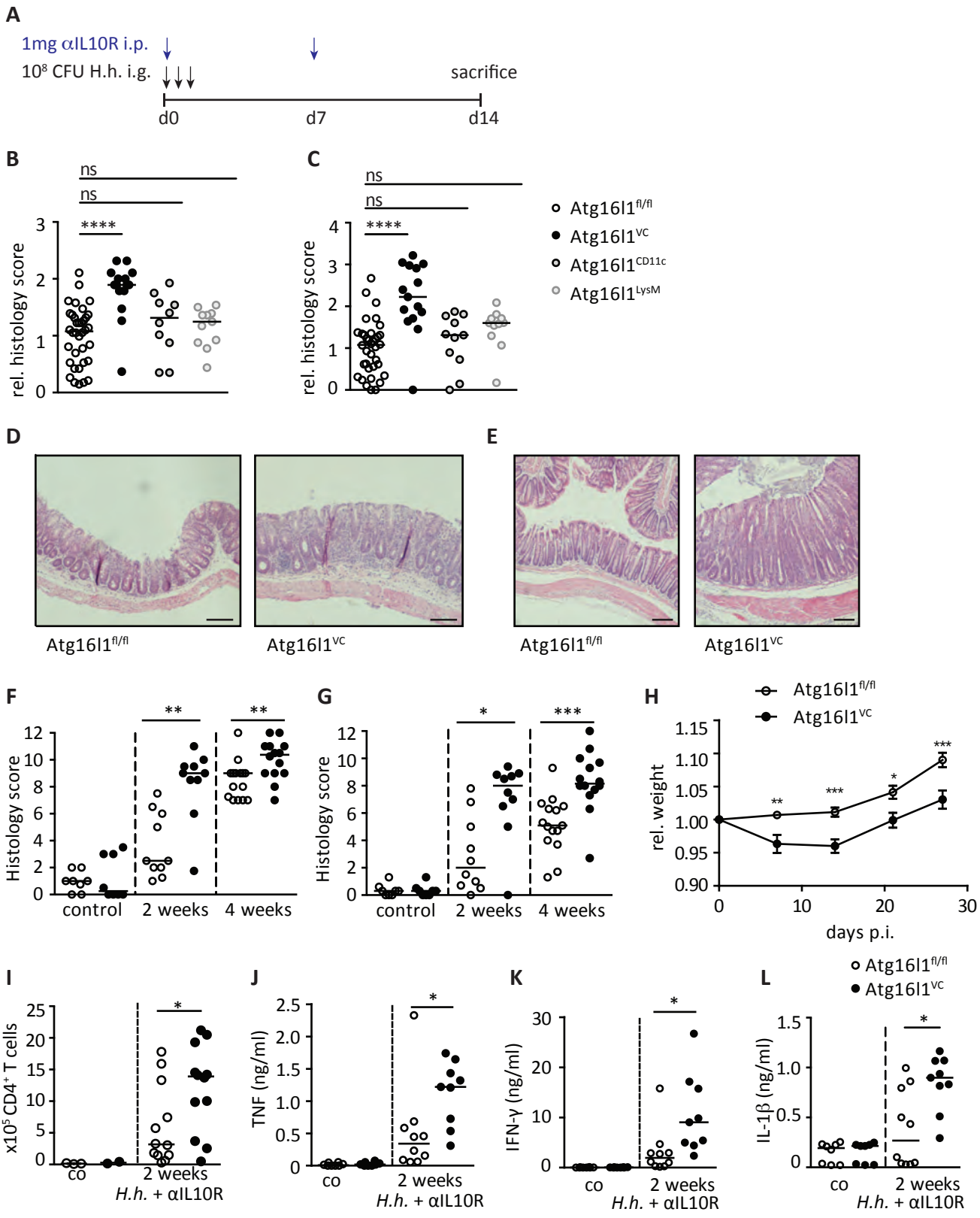
A
1mg αIL10R i.p.
10⁸ CFU H.h. i.g.
sacrifice
d0
d7
d14
B
C
ns
ns
****
rel. histology score
Atg16l1fl/fl
Atg16l1VC
Atg16l1CD11c
Atg16l1LysM
D
E
Atg16l1fl/fl
Atg16l1VC
F
G
Histology score
control
2 weeks
4 weeks
H
rel. weight
days p.i.
I
J
K
L
x10⁵ CD4⁺ T cells
TNF (ng/ml)
IFN-γ (ng/ml)
IL-1β (ng/ml)
co
2 weeks
H.h. + αIL10R

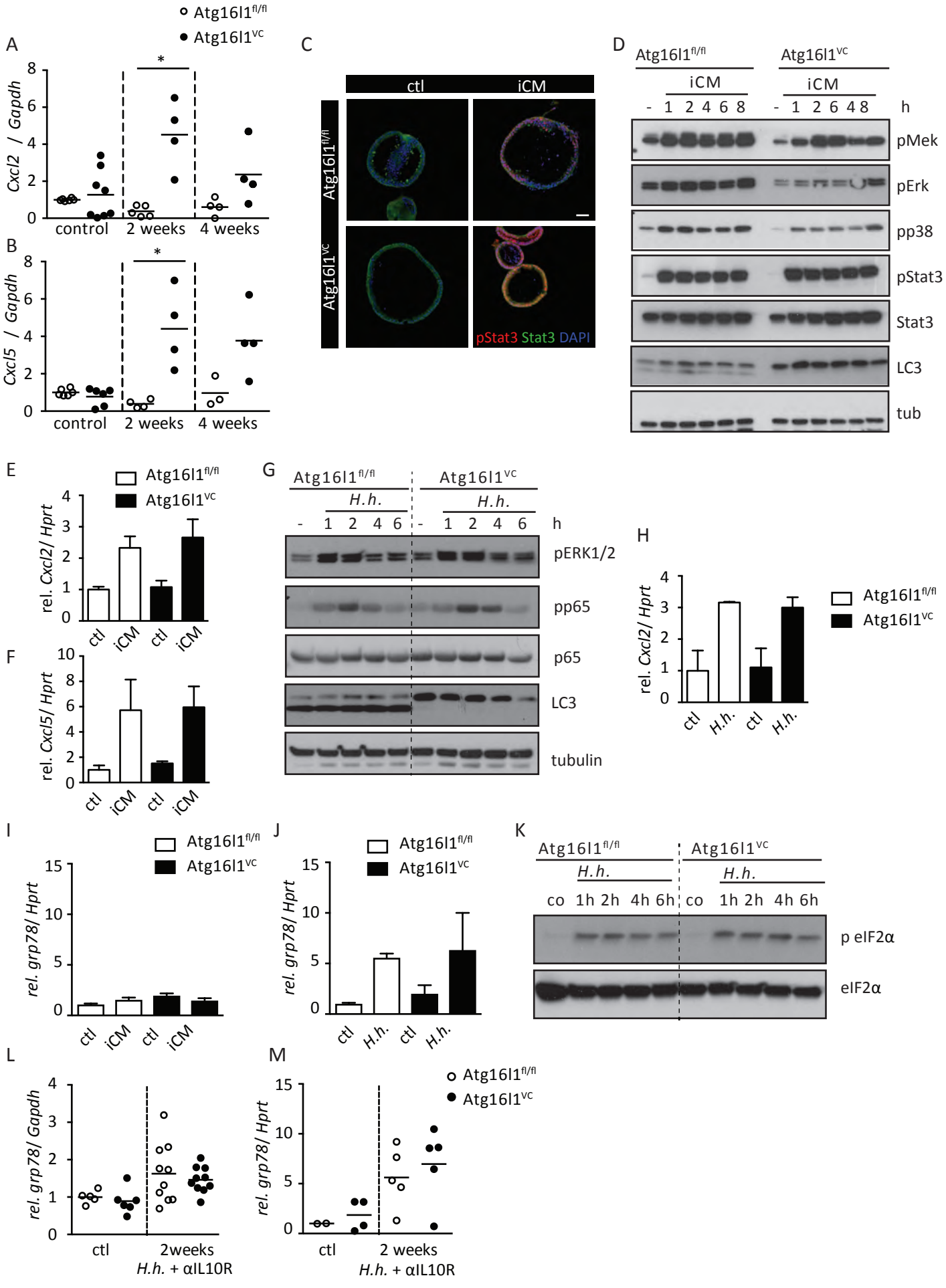
A
Atg16l1fl/fl
Atg16l1VC
Cxcl2 / Gapdh
control
2 weeks
4 weeks
B
Cxcl5 / Gapdh
C
ctl
iCM
Atg16l1fl/fl
Atg16l1VC
pStat3 Stat3 DAPI
D
Atg16l1fl/fl
Atg16l1VC
iCM
h
pMek
pErk
pp38
pStat3
Stat3
LC3
tub
E
rel. Cxcl2/ Hprt
F
rel. Cxcl5/ Hprt
G
H.h.
pERK1/2
pp65
p65
LC3
tubulin
H
I
rel. grp78/ Hprt
J
K
co
p eIF2α
eIF2α
L
rel. grp78/ Gapdh
2weeks
H.h. + αIL10R
M

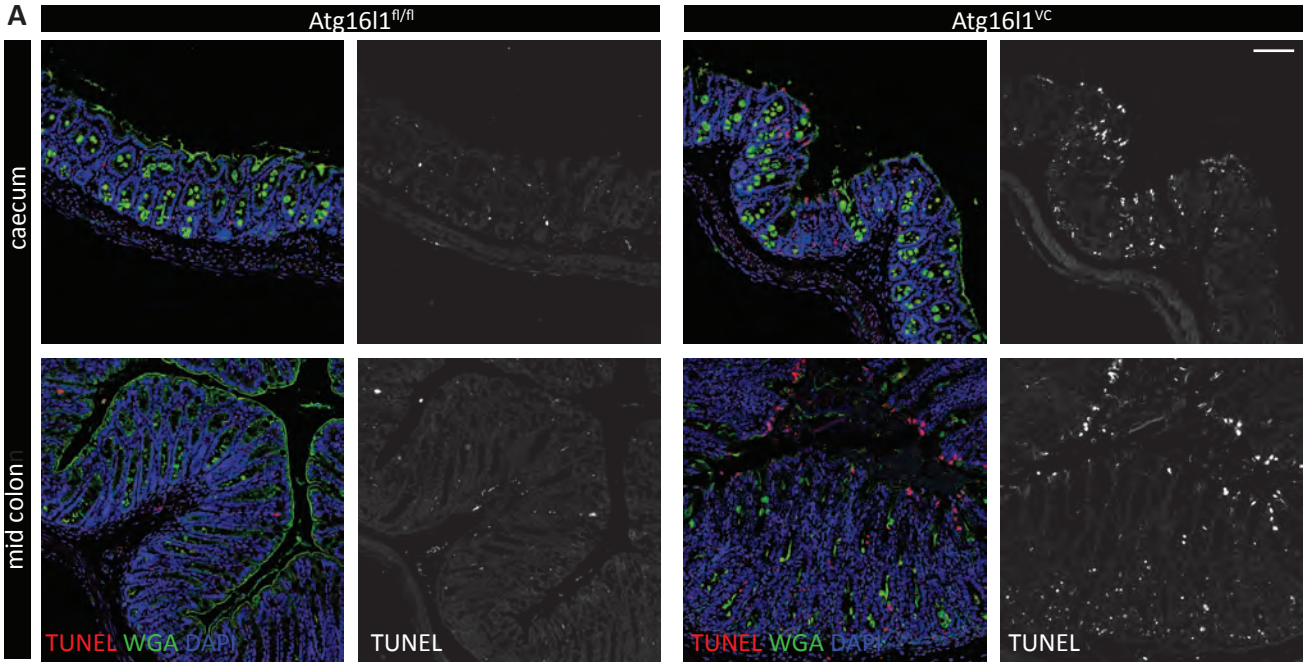
A
Atg16l1fl/fl
Atg16l1VC
caecum
mid colon
TUNEL WGA DAPI
TUNEL
TUNEL WGA DAPI
TUNEL

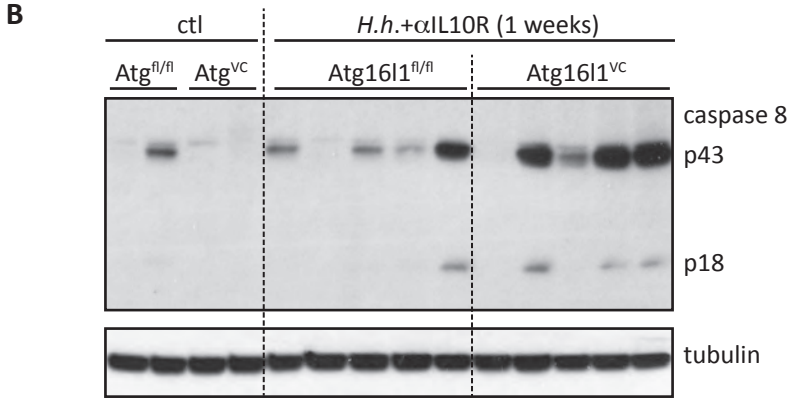
B
ctl
H.h.+αIL10R (1 weeks)
Atgfl/fl
AtgVC
Atg16l1fl/fl
Atg16l1VC
caspase 8
p43
p18
tubulin

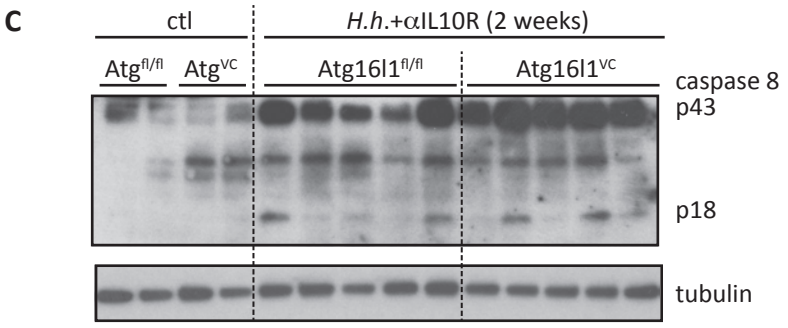
C
ctl
H.h.+αIL10R (2 weeks)
Atgfl/fl
AtgVC
Atg16l1fl/fl
Atg16l1VC
caspase 8
p43
p18
tubulin

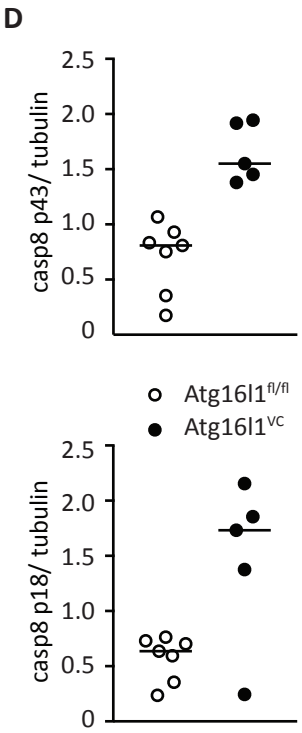
D
casp8 p43/ tubulin
2.5
2.0
1.5
1.0
0.5
0
Atg16l1fl/fl
Atg16l1VC
casp8 p18/ tubulin
2.5
2.0
1.5
1.0
0.5
0

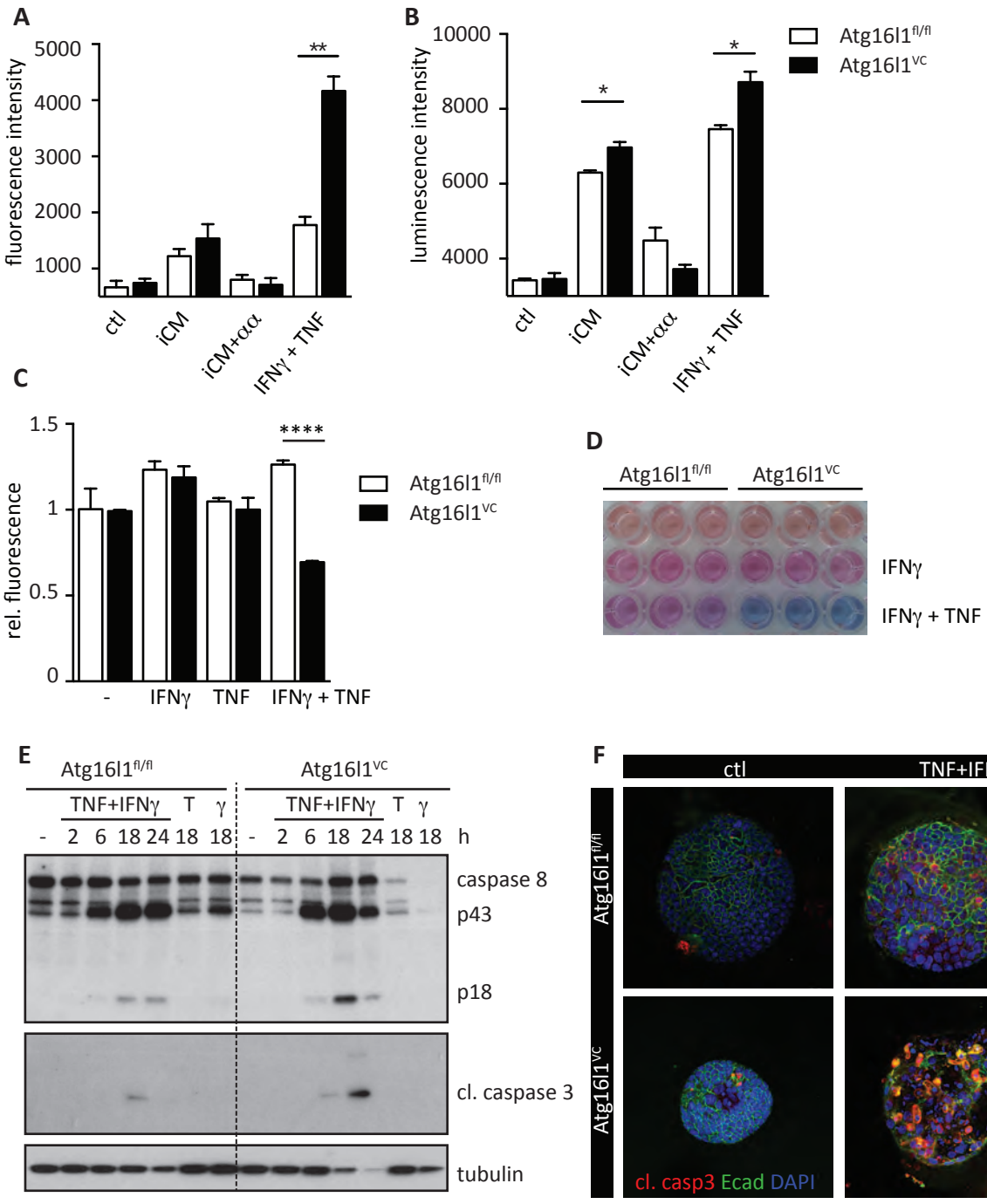
A
fluorescence intensity
5000
4000
3000
2000
1000
**
ctl
iCM
iCM+αα
IFNγ + TNF
B
luminescence intensity
10000
8000
6000
4000
*
*
Atg16l1fl/fl
Atg16l1VC
C
rel. fluorescence
1.5
1
0.5
0
****
-
IFNγ
TNF
IFNγ + TNF
D
Atg16l1fl/fl
Atg16l1VC
IFNγ
IFNγ + TNF
E
Atg16l1fl/fl
Atg16l1VC
TNF+IFNγ
T
γ
- 2 6 18 24 18 18 - 2 6 18 24 18 18 h
caspase 8
p43
p18
cl. caspase 3
tubulin
F
ctl
TNF+IFNγ
Atg16l1fl/fl
Atg16l1VC
cl. casp3 Ecad DAPI

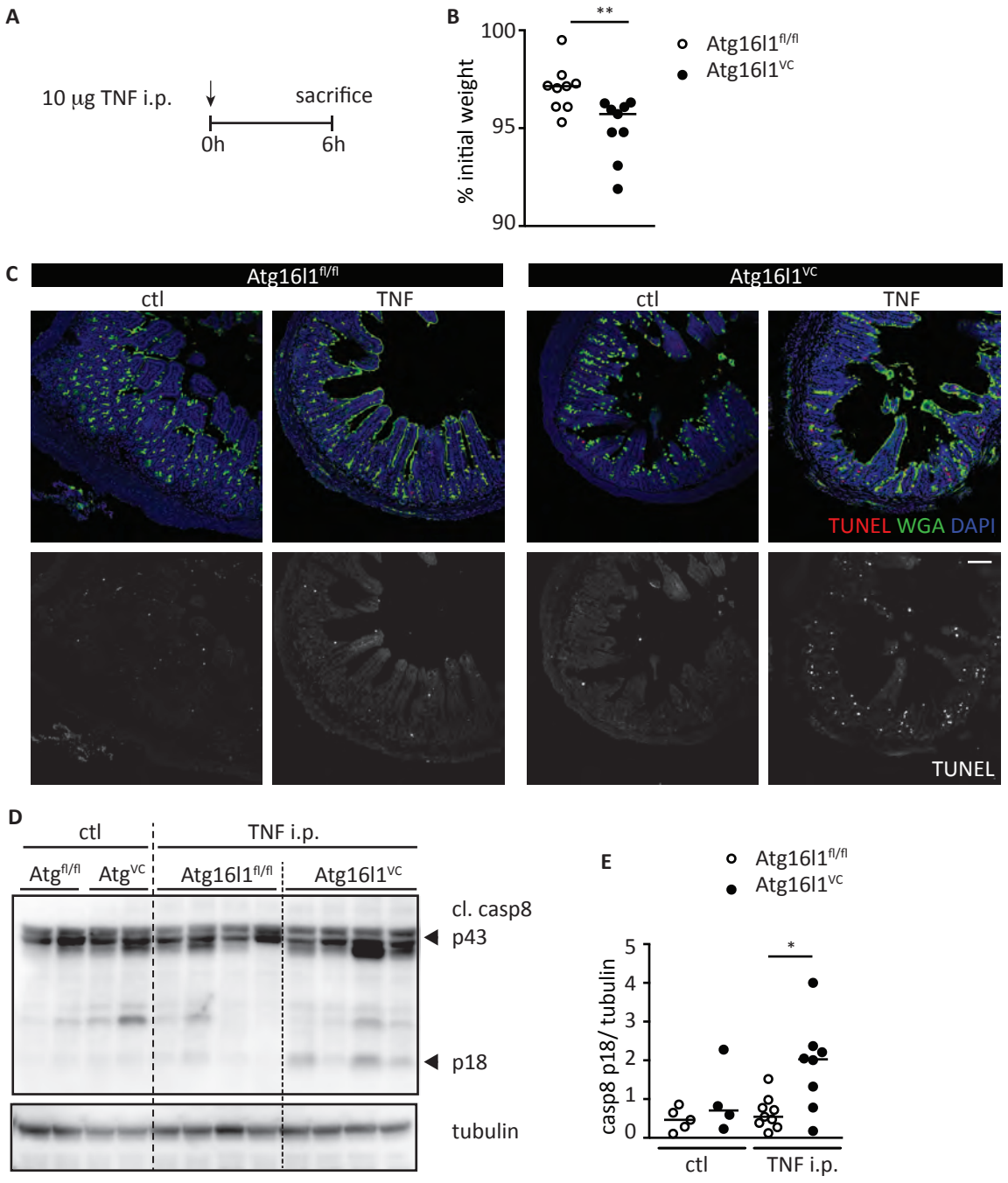
A
10 μg TNF i.p.
sacrifice
0h
6h
B
**
100
95
90
% initial weight
Atg16l1fl/fl
Atg16l1VC
C
Atg16l1fl/fl
Atg16l1VC
ctl
TNF
ctl
TNF
TUNEL WGA DAPI
TUNEL
D
ctl
TNF i.p.
Atgfl/fl
AtgVC
Atg16l1fl/fl
Atg16l1VC
cl. casp8
p43
p18
tubulin
E
Atg16l1fl/fl
Atg16l1VC
*
5
4
3
2
1
0
casp8 p18/ tubulin
ctl
TNF i.p.

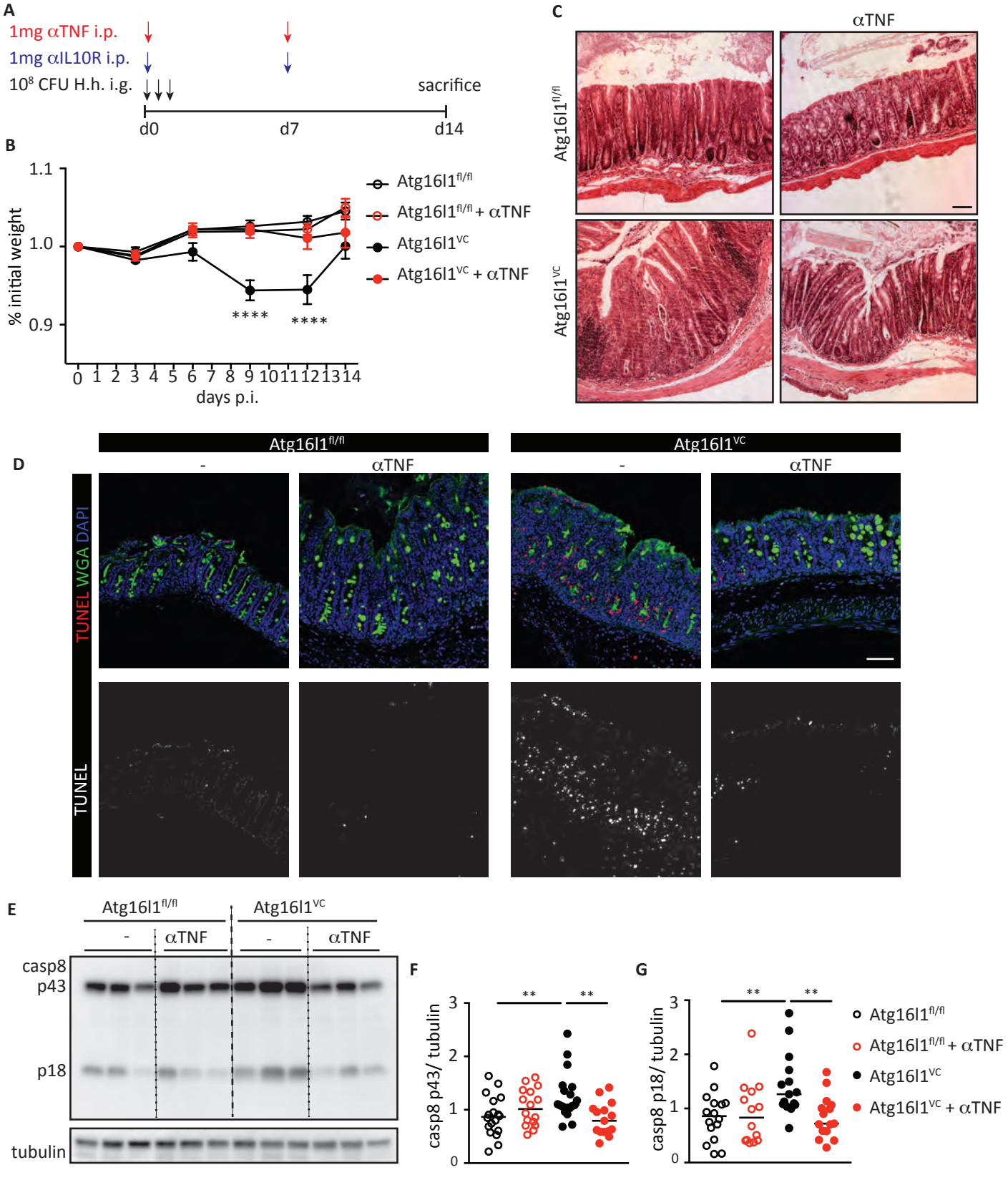
A
1mg αTNF i.p.
1mg αIL10R i.p.
10^8 CFU H.h. i.g.
sacrifice
d0
d7
d14
B
% initial weight
1.1
1.0
0.9
0 1 2 3 4 5 6 7 8 9 10 11 12 13 14
days p.i.
****
****
Atg16l1fl/fl
Atg16l1fl/fl + αTNF
Atg16l1VC
Atg16l1VC + αTNF
C
αTNF
Atg16l1fl/fl
Atg16l1VC
D
Atg16l1fl/fl
Atg16l1VC
-
αTNF
TUNEL WGA DAPI
TUNEL
E
Atg16l1fl/fl
Atg16l1VC
-
αTNF
casp8 p43
p18
tubulin
F
casp8 p43/ tubulin
**
**
G
casp8 p18/ tubulin
**
**
Atg16l1fl/fl
Atg16l1fl/fl + αTNF
Atg16l1VC
Atg16l1VC + αTNF

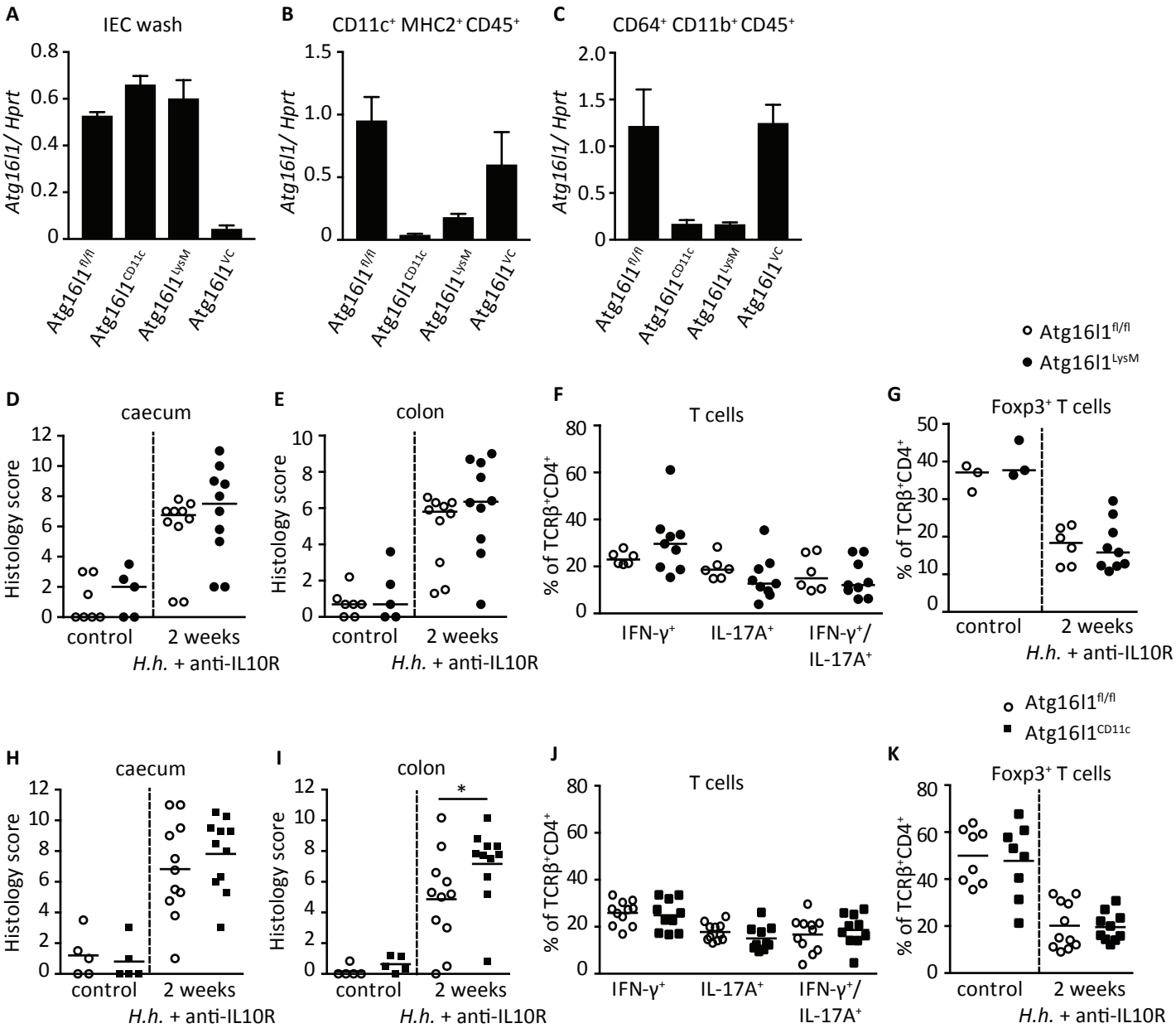

Figure S1. Related to Figure 1. Detailed analysis of *Atg16l1*^{LysM}, *Atg16l1*^{CD11c} and *Atg16l1*^{VC} mice.

A-C) Verification of *Atg16l1* deletion in distinct compartments of the intestinal mucosa in *Atg16l1*^{CD11c}, *Atg16l1*^{LysM}, *Atg16l1*^{VC} and *Atg16l1*$^{fl/fl}$ mice. qPCR analysis of *Atg16l1* expression from IEC washes (A) or on sorted DC (B) and macrophage (C) populations from LPL. *Atg16l1*^{CD11c}, *Atg16l1*^{LysM} or *Atg16l1*$^{fl/fl}$ mice were orally infected with 10^8 CFU *H.h.* on 3 consecutive days and injected with 1 mg anti-IL10R weekly and sacrificed at day 14 after colitis induction. D, E) Histopathology scores of caecum (D) and colon (E) samples from *Atg16l1*^{LysM} and *Atg16l1*$^{fl/fl}$ littermates. F) Frequencies of cytokine positive CD4$^+$TCRβ$^+$ T cells in PMA, Ionomycin re-stimulated colonic LPLs from *Atg16l1*^{LysM} and *Atg16l1*$^{fl/fl}$ littermates. G) Frequencies of Foxp3$^+$ CD4$^+$ TCRβ$^+$ T cells in colonic LPLs from *Atg16l1*^{LysM} and *Atg16l1*$^{fl/fl}$ littermates. H, I) Histopathology scores of caecum (H) and colon (I) samples from *Atg16l1*^{CD11c} and *Atg16l1*$^{fl/fl}$ littermates. J) Frequencies of cytokine positive CD4$^+$TCRβ$^+$ T cells in PMA, Ionomycin re-stimulated colonic LPLs from *Atg16l1*^{CD11c} and *Atg16l1*$^{fl/fl}$ littermates. K) Frequencies of Foxp3$^+$ CD4$^+$ TCRβ$^+$ T cells in colonic LPLs from *Atg16l1*^{CD11c} and *Atg16l1*$^{fl/fl}$ littermates.

Data are combined from 2 independent experiments (A-K). Bars represent means with SEM (A-C) or each dot represents individual mouse (D-K). Horizontal bars denote medians. Statistical significance was determined using Mann Whitney test, * $p<0.05$; *H.h.* – *Helicobacter hepaticus*, pi – post infection.

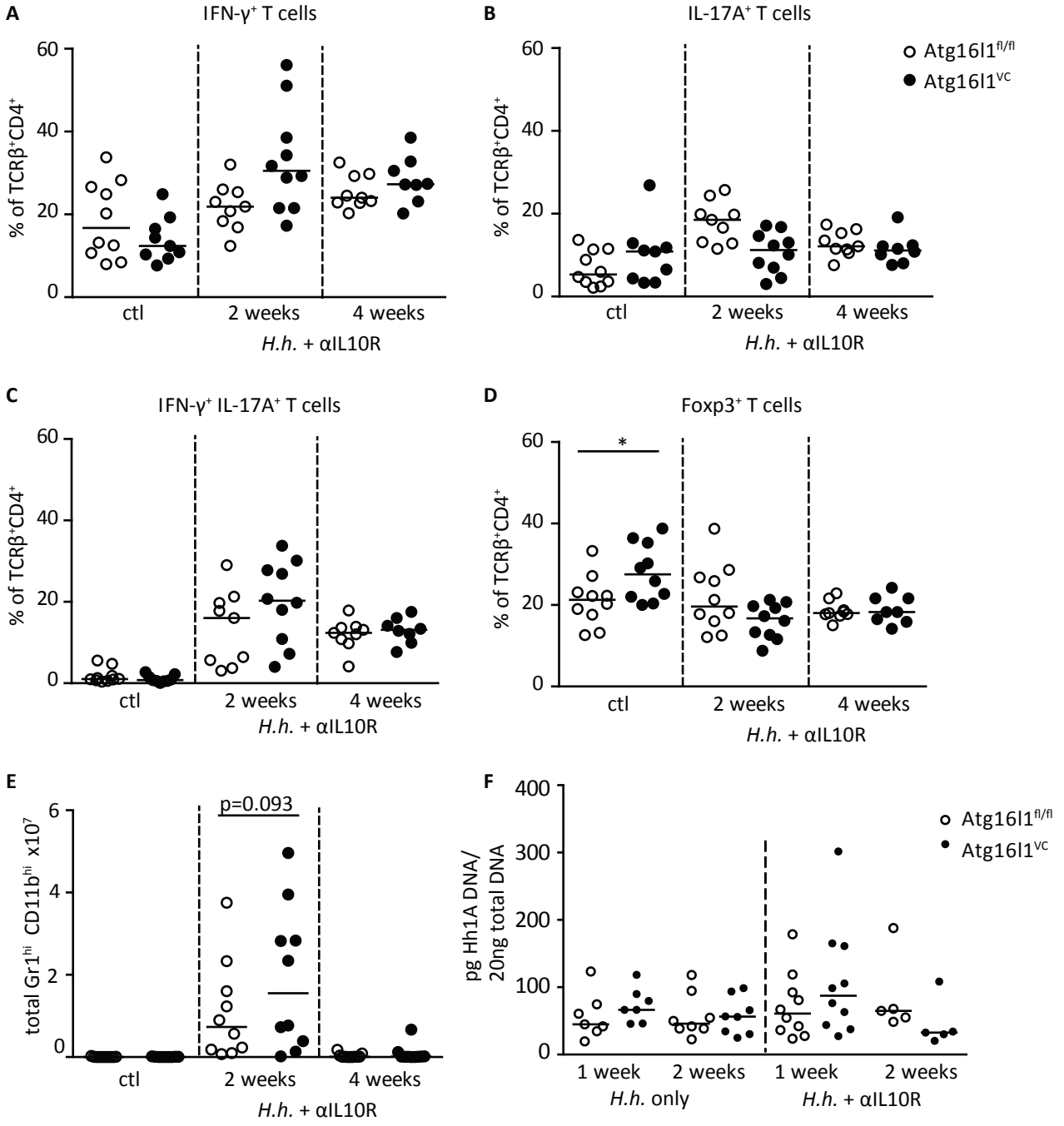

Figure S2. Related to Figure 1. Lamina propria leukocyte analysis of *Atg16l1*^{VC} mice.
Atg16l1^{VC} and *Atg16l1*$^{fl/fl}$ littermates were orally infected with 10^8 CFU *H.h.* on 3 consecutive days and injected with 1 mg anti-IL10R weekly. LPLs were analyzed by FACS at 2 weeks and 4 weeks after colitis induction. A-C) Prior to FACS staining LPLs were restimulated with PMA, Ionomycin and Brefeldin A for 3 h. Frequencies of IFN-γ$^+$ (A), IL-17A$^+$ (B) and IFN-γ$^+$/ IL17A$^+$ cells of CD4$^+$TCRβ$^+$ T cells (C). D) Frequencies of Foxp3$^+$ cells of CD4$^+$TCRβ$^+$ T cells. E) Total numbers of Gr1^{high} CD11b^{high} cells in LPLs. F) *H.h.* DNA quantities were determined by qPCR in caecal content of *Atg16l1*^{VC} and *Atg16l1*$^{fl/fl}$ littermates infected with *H.h.* only or treated with anti-IL10R weekly.

Data are combined from at least 3 independent experiments (A-E) or from 2 independent experiments (F). Each dot represents an individual mouse (A-F). Horizontal bars denote medians. Statistical significance was determined using Mann Whitney test, * $p<0.05$; ctl – control, *H.h. – Helicobacter hepaticus*, p.i. – post infection.

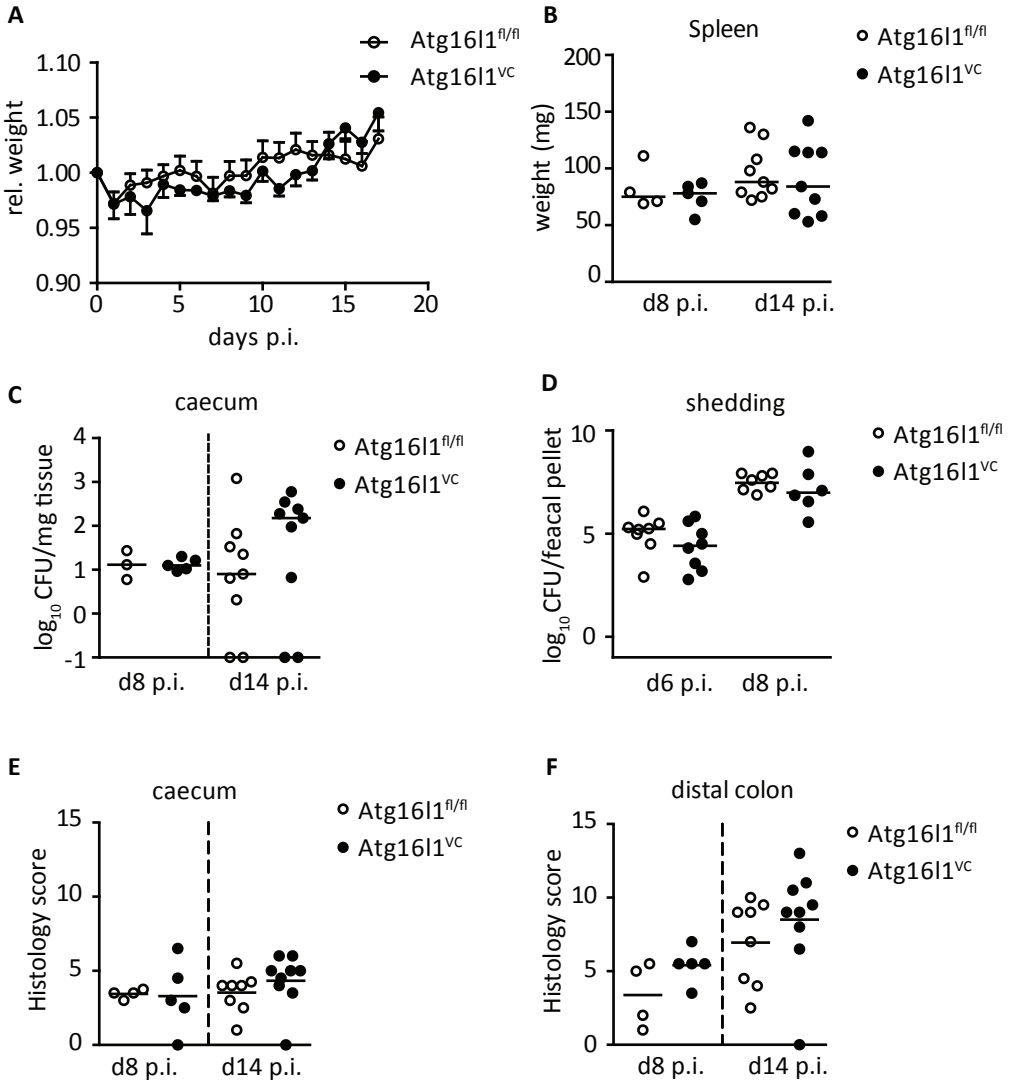

Figure S3. Related to Figure 1. *Atg16l1*^{VC} mice do not show increased susceptibility to *Citrobacter rodentium* infection.
Atg16l1^{VC} and *Atg16l1*$^{fl/fl}$ littermates were orally infected with 10^9 CFU *C. rodentium*. A) Weight was followed over 18 days. B) Spleen weights at day 8 and day 14 p.i.. C) Tissue adherent CFU in caecal tissue and D) CFU in faecal pellets of *Atg16l1*^{VC} and *Atg16l1*$^{fl/fl}$ littermates at day 8 and day 14 p.i.. E, F) Histopathology scores of the caecum (E) and distal colon (F) of *Atg16l1*^{VC} and *Atg16l1*$^{fl/fl}$ littermates at day 8 and day 14 p.i..

Data are combined from 2 independent experiments (A-F). Each dot represents an individual mouse (B-F) or mean ± S.E.M. (A). Horizontal bars denote medians. Statistical significance was determined using Mann Whitney test. CFU- colony forming units, p.i. – post infection.

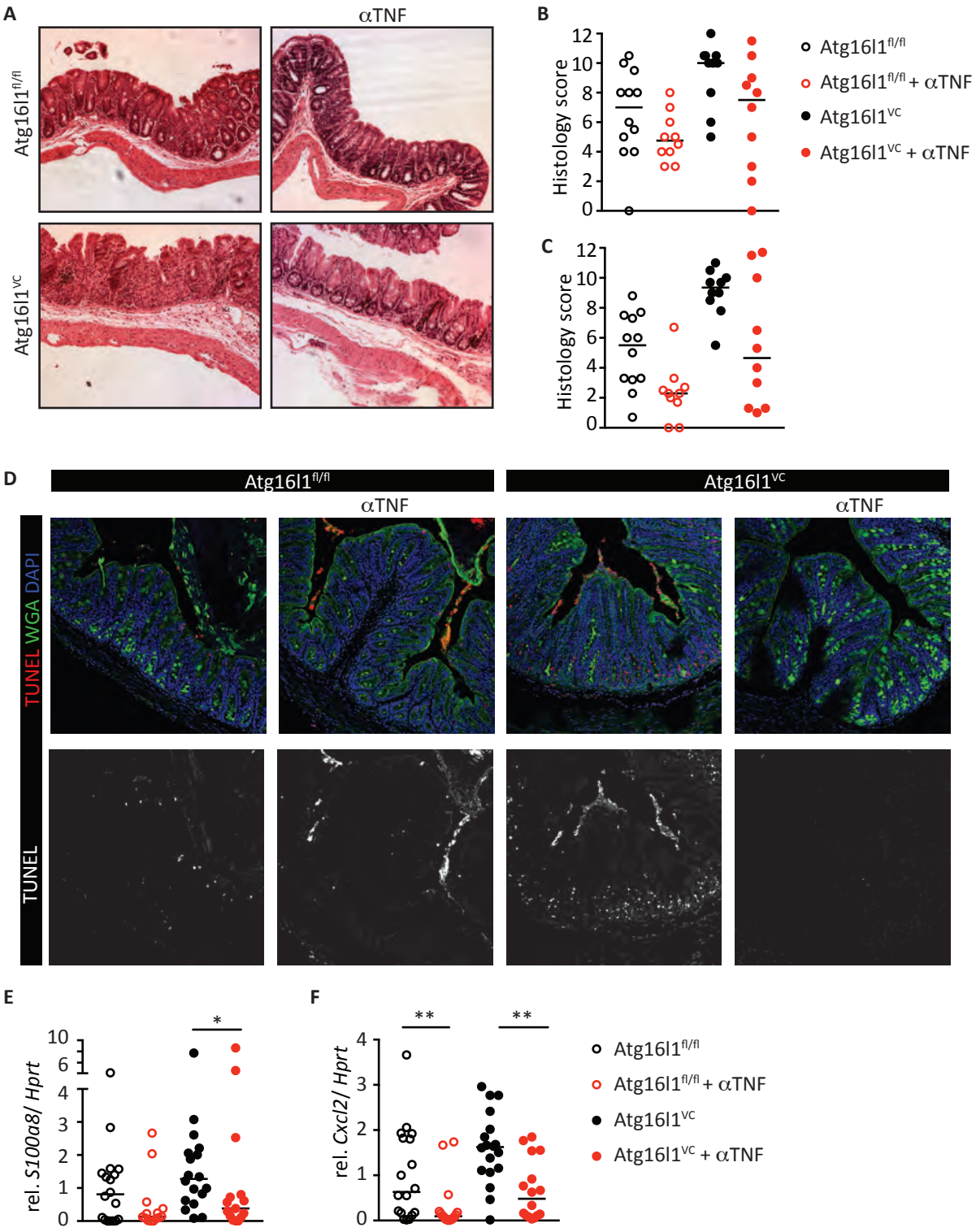

Figure S4. Related to Figure 6. TNF blockade attenuates colitis and epithelial apoptosis in *Atg16l1*^{VC} mice.
Atg16l1^{VC} and *Atg16l1*$^{fl/fl}$ littermates were orally infected with 10^8 CFU *H.h.* on 3 consecutive days and treated weekly with 1 mg anti-IL10R i.p. with indicated groups also receiving 1 mg anti-TNF i.p. at day 0 and day 6. Mice were sacrificed at day 14 after colitis induction. A) Representative micrographs of H&E stained caecal sections of *Atg16l1*^{VC} and *Atg16l1*$^{fl/fl}$ littermates. B) Histopathology scores of the caecum (B) and colon (C) of samples from *Atg16l1*^{VC} and *Atg16l1*$^{fl/fl}$ littermates. D) Representative images of TUNEL (red) staining of colon sections, counterstaining with WGA (green) and DAPI (blue). E, F) qPCR analysis of expression of *S100a8* (E) and *Cxcl2* (F) in isolated IECs from *Atg16l1*^{VC} and *Atg16l1*$^{fl/fl}$ littermates. Results were normalized to *Hprt* expression and expressed relative to the *Atg16l1*$^{fl/fl}$ group.

Data are combined (B, C, E, F) or representative (A, D) of 3 independent experiments. Each dot represents an individual mouse (B, C, E, F). Horizontal bars denote medians. Statistical significance was determined using Mann Whitney test, * $p<0.05$; ** $p<0.01$. *H.h.* – *Helicobacter hepaticus*, p.i. – post infection.

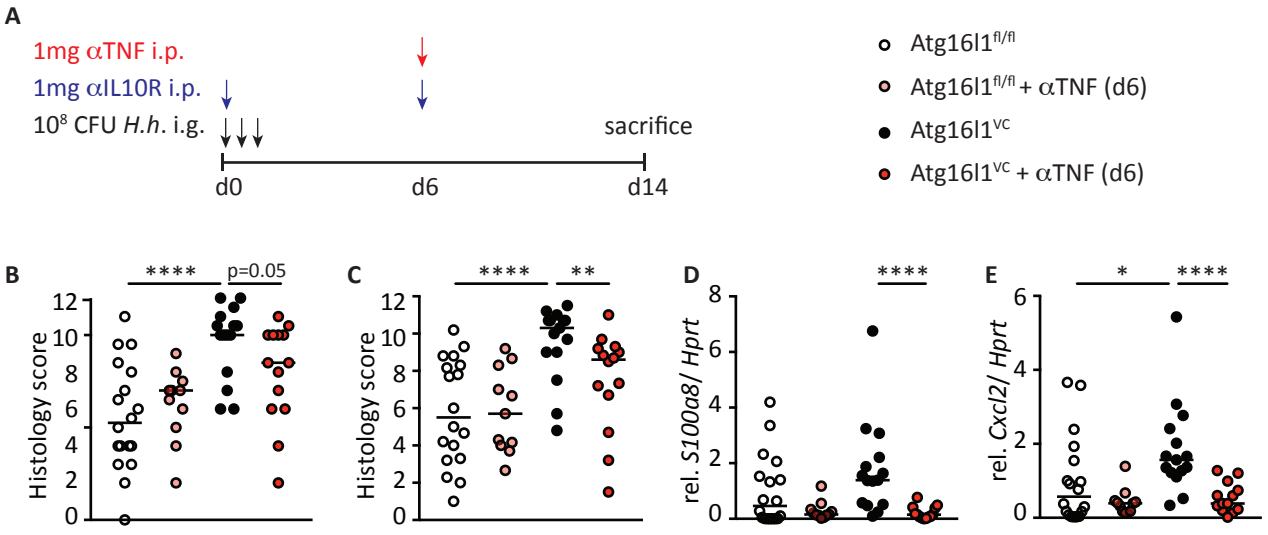

Figure S5. Related to Figure 6. αTNF therapy attenuates pathology in *Atg16l1*^{VC} mice.
Atg16l1^{VC} and *Atg16l1*$^{fl/fl}$ littermates were orally infected with 10^8 CFU *H.h.* on 3 consecutive days and treated weekly with 1 mg anti-IL10R i.p. with indicated groups also receiving 1 mg anti-TNF i.p. at day 6 after colitis induction. Mice were sacrificed at day 14 after colitis induction. A) Schematic of the treatment protocol. B,C) Histopathology scores of the caecum (B) and colon (C) samples. D,E) Gene expression analysis of isolated IECs for *S100a8* (D) and *Cxcl2* (E). Results were normalized to *Hprt* expression and expressed relative to the *Atg16l1*$^{fl/fl}$ group.

Data are combined from 3 independent experiments (B-E). Each dot represents an individual mouse (B-E). Horizontal bars denote medians. Statistical significance was determined using Mann Whitney test, * p<0.05; ** p<0.01; **** p<0.0001. *H.h. – Helicobacter hepaticus*.